UNEXPECTED SERIES OF REGULAR FREQUENCY SPACING OF δ SCUTI STARS IN THE NON-ASYMPTOTIC REGIME – II. SAMPLE – ECHELLE DIAGRAMS AND ROTATION

M. Paparó[1], J. M. Benkő[1], M. Hareter[1], and J. A. Guzik[2]

Draft version July 6, 2021

ABSTRACT

A sequence search method was developed for searching for regular frequency spacing in δ Scuti stars by visual inspection and algorithmic search. The sample contains 90 δ Scuti stars observed by CoRoT. An example is given to represent the visual inspection. The algorithm (SSA) is described in detail. The data treatment of the CoRoT light curves, the criteria for frequency filtering and the spacings derived by two methods (three approaches: VI, SSA and FT) are given for each target. Echelle diagrams are presented for 77 targets, for which at least one sequence of regular spacing was identified. Comparing the spacing and the shifts between pairs of echelle ridges revealed that at least one pair of echelle ridges is shifted to midway between the spacing for 22 stars. The estimated rotational frequencies compared to the shifts revealed rotationally split doublets, triplets and multiplets not only for single frequencies, but for the complete echelle ridges in 31 δ Scuti stars. Using several possible assumptions for the origin of the spacings, we derived the large separation ($\Delta\nu$), which are distributed along the mean density versus large separations relation derived from stellar models (Suárez et al. 2014).

Subject headings: stars: oscillations — stars: variables: Delta Scuti — techniques: photometric — space vehicles

1. INTRODUCTION

Delta Scuti stars are very complex pulsators. They are located on and above the main sequence, they pulsate mainly in p-type and g-type non-radial modes, beside the radial ones. The modes are excited by the κ-mechanism in the He ionization zone (Unno et al. 1981; Aerts et al. 2010). The amplitudes of the radial modes are remarkably lower than in the classical radial pulsators, although they lie in the extension of the classical instability strip to the main sequence. They are close to the Sun on the HR diagram, but due to the excitation of the low order modes, no high level regularity of the modes has been predicted among them. Classical pulsators, with simple structure of the excited modes, and the Sun, with stochastically excited high-order modes that are predicted to have regular frequency spacing, have the advantage for mode identification.

The space missions yielded the detection of a huge number of δ Scuti stars with a much higher signal to noise ratio than we had before (Baglin et al. 2006; Auvergne et al. 2009; Borucki et al. 2010). They allowed us the detection of a much larger set of modes. In the era of ground-based observations, we had hoped to match the increased number of modes by comparing them directly to model frequencies. Unfortunately this hope has not been realized due to the still existing discrepancy between the numbers of observed and predicted frequencies.

Up to now we could not avoid the traditionally used methods of mode identification, using the color amplitude ratio and phase differences (Watson 1988; Viskum et al. 1998; Balona & Evers 1999; Garrido 2000).

The basic problem in mode identification of δ Scuti stars is the rotational splitting of modes due to intermediate and fast rotation. Starting from the first-order effect in slow rotators (Ledoux 1951), the second-order effects (Vorontsov 1981, 1983; Dziembowski & Goode 1992) and the third-order effects (Soufi et al. 1998) were intensively investigated theoretically in the frame of the perturbative theory and were applied for individual stars (Templeton et al. 2000, 2001; Pamyatnykh et al. 1998).

The theoretical investigation of the intermediate and fast rotating stars exhibited a rapid improvement since the work of Lignières et al. (2006) and Roxburgh (2006). In the following years, a series of papers (Lignières et al. 2008, 2009, 2010; Reese et al. 2008, 2009) investigated different aspects of the ray dynamic approach for fast rotating stars. Instead of the traditional quantum numbers (l, n), they introduced the modified quantum numbers ($\hat{l}$, $\hat{n}$) including the odd and even parity of modes in fast rotating stars. They reached a level that recently echelle diagrams were published; for example, see Ouazzani et al. (2015).

In the ray dynamic approach different families of modes, named the low frequency modes, whispering gallery modes, chaotic modes and island modes were recognized. These modes represent different pulsational behavior. The low frequency modes are counterparts of the high-order g-modes. They have negligible amplitude in the outer layers, so they should not be detected observationally. The whispering gallery modes are counterparts of the high degree acoustic modes. They probe the outer layers but due to low visibility they might not be detected. Chaotic modes do not have counterparts in the non-rotating case. Due to the lack of symmetry in the cancellation and the significant amplitude in the whole of the stellar interior, these modes are expected to be detected observationally. However, they appear only in very fast rotating models. Island modes are counterparts

paparo@konkoly.hu
[1] Konkoly Observatory, MTA CSFK, Konkoly Thege Miklós út 15-17., H-1121 Budapest, Hungary
[2] Los Alamos National Laboratory, Los Alamos NM 87545 USA

of the low degree acoustic modes. They probe the outer layers of the star and present good geometric visibility. Therefore these modes should be easily detected observationally. Low $\hat{l}$ modes are expected to be the most visible modes in the seismic spectra of rapidly rotating stars. For a given parity, the mode frequencies line up along ridges of given $\hat{l}$ values. However, the first difficulty with studying the island modes is to be able to identify them among all the other type of modes present in the spectrum of rapidly rotating stars (chaotic and whispering gallery modes).

The regular arrangement of the excited modes in stars having high order p modes (Sun and solar-type oscillation in red giants) or having high order g modes (white dwarfs) allowed us to reach the asteroseismology level. The radial distribution of the physical parameters (pressure, temperature, density, sound speed and chemical composition) were derived for the Sun. The mode trapping allowed us to derive the masses of the H and He layers in white dwarfs.

Using the space data many investigations aimed to find regularity in the δ Scuti stars, in MOST data (Matthews 2007), in CoRoT data (García Hernández et al. 2009, 2013; Mantegazza et al. 2012) and in *Kepler* data (Breger et al. 2011; Kurtz et al. 2014). The most comprehensive study (García Hernández et al. 2015) reported regularities for 11 stars on a sample of 15 *Kepler* δ Scuti stars, providing the large separation for them. They revealed two echelle ridges with 6 and 4 frequency members for KIC 1571717. Up to now this is the most extended survey for regularities in δ Scuti stars.

Our goal was to survey the possible regularities of δ Scuti stars on a much larger sample of CoRoT targets. In addition, as a new method we searched for complete sequence(s) of quasi-equally spaced frequencies with two approaches, namely visual inspection and algorithmic search. We present in this paper our detailed results for the whole sample.

2. COROT DATA

The CoRoT satellite was launched in 2006 (Baglin et al. 2006). LRa01, the first long run in the direction of anti-center, started on October 15, 2007 and finished on March 03, 2008, resulting in a $\Delta T=131$ day time span. Both chromatic and monochromatic data were obtained on the EXO field with a regular sampling of 8 minutes, although for some stars an oversampling mode (32s) was applied. After using the CoRoT pipeline (Auvergne et al. 2009) the reduced N2 data were stored in the CoRoT data archive. Any kind of light curves of the EXO field were systematically searched for δ Scuti and γ Doradus light curves by one of us (Hareter 2013).

We did not rely on the automatic classification tool (CVC, Debosscher et al. 2009) because of ambiguities and the risk of misclassifications that might have appeared in the original version. Rather, we selected the targets by visual inspection of light curves and their Fourier transform and kept those for which classification spectra (AAOmega, Guenther et al. 2012; Sebastian et al. 2012) were available. A recent check of the new version of CVC (CoRoT N2 Public Archive[3],

TABLE 1
LIST OF EXCLUDED TARGETS

No	CoRoT ID	SSF	FF
16	102713193	52	−
17	102614844	78	−
42	102646094	45	−
44	102746628	51	−
57	102763839	93	−
58	102664100	35	−
59	102766985	61	−
60	102668347	123	−
61	102668428	57	−
64	102706982	68	−
41	102645677	106	14
46	102749985	63	9
85	102589213	70	10

NOTE. — The columns contain the running numbers (No), official CoRoT ID, the number of SigSpec frequencies (SSF), and the number of filtered frequencies (FF), respectively.

updated 2013 February) revealed that most of our stars (57) were classified as δ Scuti stars with high probability. Some GDOR (4), MISC (11), ACT (5) and β Ceph (3) classifications also appeared.

The initial sample of our investigation consists of 90 δ Scuti stars extracted from the early version of N2 data in the archive. Nowadays a modified version of N2 data on LRa01 can be found in the archive. Comparing our list and the new version, we noticed that the light curve of 14 stars from our initial sample had been omitted from the new version. The low peak-to-peak amplitude of the light curve, in some cases, might explain the decision but we did not find any reasons why targets with peak-to-peak amplitude from 0.01 to 0.05 mag had been excluded. We therefore kept these stars in our initial sample.

Because the CoRoT N2 data are still affected by several instrumental effects, we used a custom IDL-code that removes the outliers and corrects for jumps and trends. The jumps were detected by using a two sampled t-test with sliding samples of 50 data points and the trends were corrected by fitting low order polynomials. The outliers were clipped using an iterative median filter, where a 3σ rejection criterion was employed. The range of the light variation for most of the stars is 0.003 - 0.04 magnitude, with the highest population around 0.01 mag. The brightness range is from 12.39 to 15.12 mag, covering almost three magnitudes.

The frequencies were extracted using the software SigSpec (Reegen 2007) in the frequency range from 0 to 80 d^{-1}. The significance limit was set initially to 5. The resulting list of frequencies for 90 δ Scuti stars served as an initial database for our frequency search (Hareter 2013).

2.1. *The final sample of targets and filtering*

We filtered the SigSpec frequencies using some trivial ideas (tested for CoRoT data by Balona 2014). We removed

- low frequencies close to 0 d^{-1} in most cases up to 2 d^{-1}, since we were primarily interested in the δ Scuti frequency region

- the possible technical peaks connected to the orbital period of the spacecraft ($f_{\rm orb}$= 13.97 d^{-1})

- frequencies of lower significance in groups of closely spaced peaks, because they are most likely due to numerical inaccuracies during the pre-whitening cascade. We kept only the highest amplitude ones.

- the low-amplitude, low-significance frequencies in general. The lowest amplitude limit was different from star to star, since the frequencies showed a different amplitude range from star to star, but it was around 0.1 mmag in general.

We might dismiss true pulsating modes in the filtering process, but finding regularities among fewer frequencies is more convincing. Accidental coincidences could appear with higher probability if we use a larger set of frequencies. After finding a narrow path in solving the pulsation-rotation connection we may widen the path to a road.

In 10 stars only a few frequencies remained after the filtering process. In each case a dominant peak remained in the δ Scuti frequency range giving an excuse of the positive classification as a δ Scuti star. The limited number of frequencies in these stars was not enough for our main purpose (to find regularities between the frequencies), so we omitted them from further investigation.

In addition, we did not find any regularities in three stars. The 13 stars, that were omitted for any reason, are listed in Table 1. Our finally accepted sample where we found regularities with one of our methods is listed in Table 3. In both tables the CoRoT ID of the stars is given in the second column. For the sake of simpler treatment during the investigation we introduced a running number (first column in the tables). We refer to the stars by the running number in the rest of the paper. The 96 running numbers instead of 90 are due to a special test checking the ambiguity of our results. The double running numbers mean stars (see CoRoT ID in Table 3) where the filtering of SigSpec frequencies and the search for periodic spacing were independently done for the same stars (6 stars). The running numbers representing the same stars were identified (connected to each other) only at the end of the searching process. The independent cleaning due to the not-fixed limiting amplitude and subjectivity resulted in different numbers of the frequencies and consequently in different values of the spacing, the number of the frequencies in the echelle ridges, and the numbers of echelle ridges. The number of independent δ Scuti stars in our sample is 77, where we got positive results with one of our methods concerning the regular spacing. The $T_{\rm eff}$, $\log g$ and radial velocity ($v_{\rm rad}$), derived by one of us (Hareter 2013) are presented in the third, fourth and fifth column of Table 3.

The filtering guidelines yielded a much reduced number of frequencies. For comparison we listed the number of SigSpec frequencies (SSF) and that of the filtered frequencies (FF) in the 6th and 7th columns. Only about 20-30% of the original peaks were kept in our final list of frequencies. When the effectiveness of our method for finding regularities has been confirmed, the application could be extended including frequencies at lower amplitude. For possible additional investigation we attached

the filtered frequencies of each star to this paper in an electronic version[4]. Table 2 shows an excerpt from this data file as an example. Additional information on flags is discussed later.

3. SEARCH FOR PERIODIC SPACING

Investigations on the regular behavior of frequencies in δ Scuti stars and derivation of the large separation have been carried out in the past (see in Paparó et al. 2015). Even in the earlier years clustering of non-radial modes around the frequencies of radial modes over many radial orders has been reported for a number of δ Scuti stars: 44 Tau, BL Cam, FG Vir (Breger et al. 2009), giving the large separation. The clustering supposes that the sequence of low-order l=1 modes, slightly shifted with respect to the frequency of the radial modes, also reveals the large separation in the mean value (Breger et al. 1999). In all cases the histogram of the frequency differences or the Fourier Transform (FT) using the frequencies as input data were used. Both methods are sensitive to the most probable spacing frequency differences.

We searched for sequence(s) among the frequencies with quasi-equal spacing in our sequence search method. The visual inspection (VI) of our targets in the whole sample led us to establish the constraints for the Sequence Search Algorithm (SSA). We present here the description of both the VI and the SSA and the results for the individual targets.

3.1. Visual inspection (VI)

In the visual inspection of the frequency distribution of our target, we recognized that almost equal spacing exists between the pair(s) of frequencies of the highest amplitude. The pairs proved to be connected to each other producing a sequence. New members with frequencies of lower amplitude were intentionally searched, so the sequence was extended to both the lower and higher frequency regions. Following the process with other pairs of frequencies of higher amplitude, we could localize more than one sequence, sometimes many sequences in a star. We noticed such an arrangement from star to star over the whole sample. We present here another example of the sequences compared to Paparó et al. (2015) (paper Part I), to show how equal the spacings are between the members of a sequence, how the sequences are arranged compared to each other, and how we find a sequence if one consecutive member is missing. A new parameter appears in this process, namely the shifts of a frequency (member) to the consecutive lower and higher frequencies of the reference sequence (the first one is accepted).

Fig. 1 shows four sequences of similar regular spacing for CoRoT 102670461 (running number: 65). The sequences consist of 8, 6, 4 and 4 members, respectively, altogether including more than 45% of the filtered frequencies. We allowed to miss one member of the sequence, if the half of the second consecutive member's spacing matched the regular spacing. In this particular case the missing members of the sequences are in the 20-23.5 d^{-1} interval, which is in general the middle of the interval of the usually excited modes in δ Scuti stars. The frequencies of the highest amplitudes normally appear in
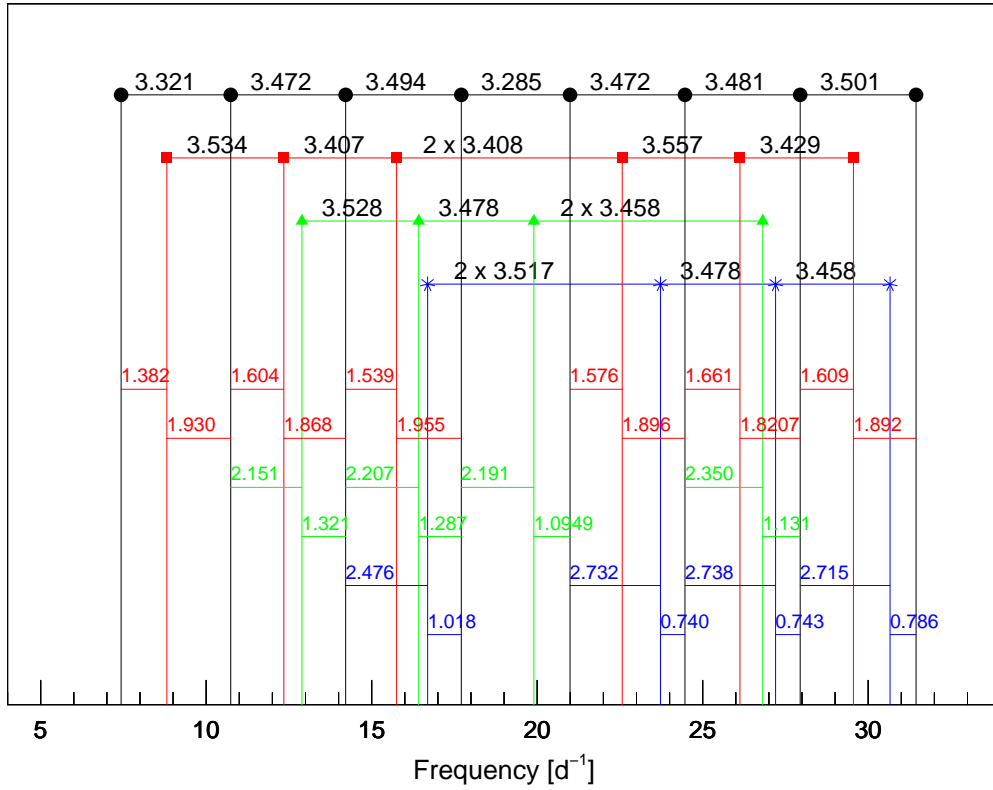
---

[4] See the web page of this journal: `http://`

Fig. 1.— Sequences with quasi-equal spacing, and shifts of the sequences for star No. 65 (CoRoT 102670461). 1st – black dots, average spacing 3.431 ± 0.091 d^{-1}; 2nd – red squares, 3.467 ± 0.073 d^{-1}; 3rd – green triangles, 3.488 ± 0.036 d^{-1}; 4th – blue stars, 3.484 ± 0.030 d^{-1} average spacings were obtained. The mean spacing of the star is 3.459 ± 0.030 d^{-1}. The shifts of the 2nd, 3rd and 4th sequences relative to the first one are also given in the same color as the sequences.

TABLE 2
SAMPLE FROM THE DATA FILE

No	CoRoT ID	f (d^{-1})	$A(f)$ (mmag)	VI1	VI2	SSA1	SSA2	SSA3
1	102661211	10.0232	8.462	0	—	1	1	—
1	102661211	7.8170	3.606	2	—	2	5	—
1	102661211	14.7389	1.990	3	—	6	0	—
1	102661211	12.0054	1.602	6	—	2	4	—
1	102661211	8.7854	1.437	5	—	4	0	—
...	...	...	...	...	...	...	...	...

NOTE. — This table is published in its entirety in the electronic edition of ApJS, a portion is shown here for guidance regarding its form and content. The columns contain local id, CoRoT ID, used frequency, Fourier amplitude of the frequency, and echelle ridge flags of the frequency obtained from the different search methods (VI or SSA), respectively. The 0 value means that the frequency is not on any echelle ridges, while sign − denotes nonexistent search result. See the text for details.
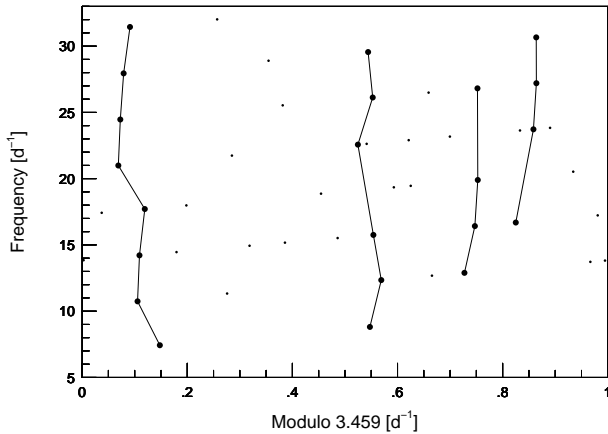
FIG. 2.— Echelle diagram of the star No. 65, consistent with the four sequences of Fig. 1. 45% of the filtered frequencies are located on the echelle ridges (the other frequencies are shown by small dots).

this region. The mean value of the spacing is independently given for each sequence in the figure's caption. The mean values differ only in the second digits. The general spacing value, calculated from the average of the sequences, is 3.459 ± 0.030 d^{-1}.

Fig. 1 also displays the shifts that we discussed before. They do not have random value, but represent characteristic values. Although the shifts are not the same for each member in a sequence, their mean values are characteristic for each sequence. We got 1.562 ± 0.097 and 1.894 ± 0.047 for the second, 2.225 ± 0.087 and 1.208 ± 0.112 for the third and 2.665 ± 0.127 and 0.821 ± 0.132 d^{-1} for the fourth sequence relative to the first (reference) sequence. The frequencies of the second sequence are almost midway between the first sequence, which we would expect in a comb-like structure. The third sequence is shifted by 0.635 d^{-1} relative to the second one, while the fourth one is shifted by 0.297 d^{-1} relative to the third one (practically half of the shift between the second and third sequences) although this value is determined only by averaging two independent values due to the missing members in the sequences. The shift of the fourth sequence relative to the second one is 1.069 d^{-1}.

According to the AAO spectral classification (Guenther et al. 2012; Sebastian et al. 2012), CoRoT 102670461 has $T_{\mathrm{eff}}=7325 \pm 150$ K, $\log g=3.575 \pm 0.793$ and A8V spectral type and a variable star classification as a δ Scuti type star (Debosscher et al. 2009). Following the process used by Balona et al. (2015) for *Kepler* stars (discussed later in detail), we derived a possible equatorial rotational velocity (100 km s^{-1}) and a first-order rotational splitting (0.493 d^{-1}). Knowing the rotational splitting another regularity appears. The shift of the fourth sequence relative to the second one (1.069 d^{-1}) remarkably agrees with twice the value of the estimated equatorial rotational splitting. The appearance of twice the value of the rotational frequency is predicted by the theory (Lignières et al. 2010).

The sequences in Fig. 1 are practically a horizontal representation of the widely used echelle diagram. In Fig. 2

we present the echelle diagram of the star No. 65, modulo 3.459 d^{-1}, in agreement with Fig. 1. Fig. 2 displays all the filtered frequencies (small and large dots) but only 45% of them are located on the echelle ridges (large dots). The first, second, third and fourth sequences in the order of Fig. 1 agree with the echelle ridges at about 0.1, 0.55, 0.75 and 0.85 d^{-1}, respectively, in modulo value.

We found sequence(s) in 65 independent targets by the visual inspection. The number of frequencies included in the sequences (EF$_{\mathrm{VI}}$), the number of sequences (SN$_{\mathrm{VI}}$) and the spacings (SP$_{\mathrm{VI}}$) are given in the 8th, 9th and 10th columns of Table 3, respectively. To archive the work behind these columns we added flags in five additional columns to the frequencies of the sequences in the electronic table (see also Table 2). Concerning a given star, many columns contain flags, as many spacing values were found by our methods. VI means the sequence of the visual inspection, while $1, 2, \ldots,$ flag means that this frequency belongs to the 1st, 2nd, ..., sequence. The 0 flag marks those frequencies that are not located in any sequence. If the visual inspection resulted in more than one spacing, then VI1 and VI2 columns were filled in. Using the flagged frequencies a similar diagram could be prepared for all targets, obtaining the individual spacings and the shifts which we presented in Fig. 1 for the star No. 65. The distribution of the spacing obtained by visual inspection on the whole sample shows two dominant peaks between 2.3-2.4 d^{-1} (10 stars) and an equal population between 3.2-3.5 d^{-1} (7, 7 and 6 stars in each 0.1 d^{-1} bins).

We summarize the results on the independent spacings as follows. The ambiguity of the personal decision is shown by six cases (double numbering), where both the filtering process and the visual inspection were independently done. The most serious effect probably was the actual personal condition of the investigator. Since we do not want to polish our method we honestly present the differences in the solution. Different EF$_{\mathrm{VI}}$, SN$_{\mathrm{VI}}$ and sometimes different spacing (SP$_{\mathrm{VI}}$) values were derived. However, in half of the cases the independent investigation resulted in similar spacing (stars No. 1=55, 2=66 and 8=92). In two stars one of the searches had negative results (stars No. 81 and 13) while the other search was positive (stars No. 11 and 74). There was only one case (star No. 14=96) where a completely different spacing value was obtained (1.844 versus 2.429, 3.3387 d^{-1}). In a few cases (stars No. 50, 54 and 77) a spacing and twice its value were also found. However, those cases are more remarkable (stars No. 78, 92 and 96), where both of the two most popular spacings were found. They argue against the simplest explanation, namely that the sequences represent the consecutive radial order with the same l value.

The visual inspection is not the fastest way for searching for regular spacing in a large sample. We developed an algorithmic search using the constraints that we learned in the visual inspection as a first trial on the long way to disentangling the pulsation and rotations in δ Scuti stars. Following this concept we could test that the sequence search algorithm (SSA) properly works. Any extension could come only after the positive test of the first trial.

3.2. *The Algorithm (SSA)*

We present here the Sequence Search Algorithm (SSA) developed for treatment of an even larger sample than ours. We define the ith *frequency sequence* for a given star with n element by the following set: $S_i = \{f^{(1)}, f^{(2)}, f^{(3)}, \ldots, f^{(n)}\}$, where i and n are positive integers $(i, n \in \mathbb{N})$. The S_i set is ordered $\{f^{(1)} < f^{(2)} < \ldots < f^{(n)}\}$ and

$$f^{(j)} + kD - \Delta f \leq f^{(j+1)} \leq f^{(j)} + kD + \Delta f \quad (1)$$

is true for each $(f^{(j)}, f^{(j+1)})$ pair, $j \in \mathbb{N}$, $k = 1$ or $k = 2$. D means the *spacing*, Δf is the *tolerance value*. The upper frequency indices indicate serial numbers within the found sequence. We define independent lower frequency indices as well which show the position in the frequency list ordered by decreasing amplitude vis. $A(f_1) > A(f_2) > A(f_3), \ldots,$.

Since we do not have definite knowledge that all modes are excited above an amplitude limit, we allowed "gaps" in the sequences. This means that the sequence's definition inequality Eq. (1) is fulfilled for some j indices at $k = 2$. Formulating this in another way, $S_i = \{f^{(1)}, f^{(2)}, \ldots, f^{(j)}, \emptyset, f^{(j+1)}, \ldots, f^{(n)}\}$ is considered as a sequence, where $\emptyset$ means the empty set. We also allow more than one gaps in a sequence, but two subsequent gaps are forbidden.

TABLE 3
LIST OF OUR SAMPLE

No	CoRoT ID	T_{eff} (K)	$\log g$	v_{rad} (km s^{-1})	SSF	FF	EF_{VI}	SN_{VI}	SP_{VI} (d^{-1})	EF_A	SN_A	SP_A (d^{-1})	SP_{FT} (d^{-1})
1=55	102661211	7075	3.575	45.0	163	52	25	6	2.251	28,29	6,5	2.092,1.510	0.886
2=66	102671284	8550	3.650	87.5	130	19	8	1	2.137	5	1	2.161	2.137
3	102702314	7000	2.975	95.0	141	25	12	3	2.169	10	2	2.046	0.933
4	102712421	7400	3.950	32.5	103	25	13	2	2.362	11	2	2.356	2.294
5	102723128	6975	3.900	2.5	72	18	7	2	1.798	8	2	1.668	1.852
6	102703251	9100	3.800	42.5	118	27	6	1	1.850	15	3	1.767	1.866
7	102704304	7050	3.250	55.0	184	53	–	–	–	30	6	1.795	0.779
8=92	102694610	8000	3.700	55.0	193	55	14	3	2.470	35	8	2.481	4.237
9	102706800	7125	3.325	52.5	122	49	27	5	2.758	21,22	4,5	2.784,3.506	1.786
10	102637079	7325	3.850	35.0	162	43	21	3	2.629	21	4	2.614	1.374
11=81	102687709	7950	4.400	47.5	107	19	9	2	3.481	5	1	3.570	3.472
12	102710813	8350	4.150	70.0	94	13	4	1	2.573	4	1	2.569	3.125
13=74	102678628	7100	3.225	45.0	230	49	–	–	–	16	4	2.674	2.809
14=96	102599598	7600	4.000	65.0	99	18	4	1	1.844	5	1	1.866	3.472
15	102600012	8000	4.400	12.5	107	27	9	1	2.475	4,4	1,1	7.342,2.438	2.809
18	102618519	7500	4.500	35.0	102	54	10	1	2.362	18,11,16	4,2,3	6.001,2.359,3.345	2.232
19	102580193	7525	4.150	50.0	125	43	7	1	3.531	8,8	2,2	6.175,4.023	3.205
20	102620865	11250	3.975	50.0	244	40	–	–	–	19	4	1.974	1.097
21	102721716	7700	4.150	25.0	149	52	21	3	2.537	9,5	2,1	7.492,2.636	2.427
22	102622725	6000	4.300	−20	144	23	15	4	3.497	5,5	1,1	1.877,2.598	4.464
23	102723199	6225	3.225	40.0	113	22	9	3	3.364	10	2	1.461	1.316
24	102623864	7900	4.000	50.0	117	30	16	4	2.226	8	2	3.320	2.294
25	102624107	8400	4.050	57.5	70	32	4	1	3.215	8	2	3.299	2.100
26	102724195	7550	3.900	42.5	58	28	14	3	3.362	10,9	2,2	3.200,2.728	1.208
27	102728240	7450	4.200	25.0	168	55	20	4	3.255	18,18	4,4	5.995,3.178	1.623
28	102702932	6975	3.350	47.5	155	48	16	4	3.247	26	6	2.655	0.806
29	102603176	12800	4.300	35.0	308	64	29	6	2.342	35	7	2.389	0.984
30	102733521	7125	3.625	50.0	174	43	18	3	3.267	16,17	4,3	3.437,2.297	1.667
31	102634888	7175	4.000	40.0	179	39	–	–	–	15	3	2.622	1.344
32	102735992	7225	3.800	62.5	83	38	10	2	3.117	16	4	3.253	1.552
33	102636829	7000	3.200	42.5	93	43	9	2	2.303	21,23	5,5	2.396,1.540	1.282
34	102639464	9450	3.900	52.5	141	31	–	–	–	5	1	3.099	3.333
35	102639650	7500	3.900	32.5	78	28	16	3	3.484	8,9	2,2	3.492,2.609	3.387
36	102641760	7950	4.300	40.0	135	32	–	–	–	9	2	2.723	2.632
37	102642516	7275	3.700	45.0	72	20	8	2	2.335	5	1	2.586	3.012
38	102742700	7550	3.875	15.0	121	28	14	3	2.443	5	1	2.910	2.404
39	102743992	7950	4.300	42.5	126	20	6	1	2.454	6	1	4.382	4.386
40	102745499	7900	3.850	80.0	119	22	10	3	2.603	8	2	1.747	1.323
43	102649349	9425	3.950	65.0	121	16	4	1	1.949	5	1	1.947	2.119
45	102647323	8200	4.300	67.5	100	32	7	1	2.379	8,9	2,2	3.306,1.407	3.846
47	102650434	8500	3.875	72.5	210	34	13,14	3,4	1.597,2.525	11	2	1.611	1.092
48	102651129	8350	3.750	40.0	88	35	12	2	3.413	13	3	3.464	3.521
49	102753236	7600	4.100	32.5	375	37	12	2	3.767	14	3	2.317	2.604
50	102655408	7375	4.000	42.5	75	28	14,6	3,1	3.394,1.550	8	2	3.936	2.747
51	102655654	7200	3.675	72.5	97	16	4	1	3.377	4	1	1.867	3.378
52	102656251	7950	4.200	60.0	128	22	4	1	3.288	10	2	2.747	1.623
53	102657423	8150	3.425	52.5	161	36	10	2	2.523	18	4	2.492	2.403
54	102575808	7250	3.325	17.5	202	47	22,37	4,6	4.659,2.289	17,18	4,4	2.300,3.275	4.717
55=1	102661211	7075	3.575	45.0	163	43	9	3	2.337	21,24	5,5	2.544,2.262	0.874
56	102761878	7375	3.700	32.5	80	11	4	1	2.564	–	–	–	4.310
62	102576929	8925	4.050	32.5	104	20	7	2	6.365	9	2	1.834	1.748
63	102669422	7300	3.675	50.0	82	35	14	2	3.390	18	4	3.285	1.712
65	102670461	7325	3.575	50.0	142	49	22	4	3.459	21	4	3.437	1.282
66=2	102671284	8550	3.650	87.5	130	39	10	2	2.152	16	4	2.406	2.119
67	102607188	8100	4.200	40.0	95	23	–	–	–	4	1	3.101	3.425

TABLE 3 — *Continued*

No	CoRoT ID	$T_{\rm eff}$ (K)	$\log g$	$v_{\rm rad}$ (km s^{-1})	SSF	FF	EF$_{\rm VI}$	SN$_{\rm VI}$	SP$_{\rm VI}$ (d^{-1})	EF$_{\rm A}$	SN$_{\rm A}$	SP$_{\rm A}$ (d^{-1})	SP$_{\rm FT}$ (d^{-1})
68	102673795	8050	3.750	27.5	65	13	–	–	–	5	1	1.929	2.119
69	102773976	7525	4.400	17.5	52	13	–	–	–	4	1	4.682	3.731
70	102775243	7950	4.250	50.0	126	31	10,4	2,1	4.167,3.002	8	2	3.059	3.676
71	102775698	9550	3.750	22.5	473	56	24	4	3.351	30,28	6,6	3.277,2.218	1.131
72	102675756	7350	3.175	77.5	342	40	23	4	2.277	23,25	5,5	2.249,1.977	2.137
73	102677987	7700	3.950	37.5	102	26	13	3	3.293	8,10	2,2	3.416,2.417	1.176
74=13	102678628	7100	3.225	20.0	230	68	32	6	3.343	37	8	2.940	0.647
75	102584233	6400	3.725	75.0	58	12	6	2	3.287	–	–	–	3.472
76	102785246	7425	3.800	30.0	76	37	20	5	3.527	21,21	4,4	1.772,2.067	1.761
77	102686153	7125	3.525	45.0	106	31	10,19	2,6	2.867,5.713	9,9	2,2	2.521,3.692	2.033
78	102786753	7100	3.425	55.0	238	59	22,11	4,2	2.543,3.297	29	6	2.392	1.101
79	102787451	7300	4.000	37.5	76	13	6	2	3.428	4	1	3.357	3.676
80	102587554	7375	3.700	47.5	82	34	13,14	3,2	4.293,2.487	11,15,12	2,3,3	4.247,1.734,3.365	1.712
81=11	102687709	7950	4.400	47.5	107	36	–	–	–	8	2	3.480	4.032
82	102688156	7725	4.400	55.0	96	21	7	1	2.308	5	1	4.098	4.032
83	102788412	8000	3.925	70.0	47	10	5	1	2.357	–	–	–	6.250
84	102688713	7300	4.150	47.5	111	40	4	1	3.584	17	4	2.699	2.500
86	102589546	7250	3.700	27.5	178	35	17	3	2.599	13,12	3,2	4.890,2.591	2.551
87	102690176	7425	3.525	60.0	111	35	20	4	2.551	17	4	1.458	4.386
88	102790482	7225	3.475	52.5	125	48	15	3	2.704	19	4	2.837	2.358
89	102591062	7600	3.650	30.0	101	10	6	1	2.551	–	–	–	6.944
90	102691322	7650	4.050	37.5	45	18	–	–	–	4,4	1,1	7.170,3.645	3.497
91	102691789	7800	3.750	75.0	58	20	9	2	2.648	5	1	2.803	6.250
92=8	102694610	8000	3.700	55.0	193	53	30,22	5,5	2.454,3.471	35,38	7,7	2.576,1.880	4.032
93	102794872	7575	4.150	32.5	157	58	8	1	4.346	20	4	4.219	1.706
94	102596121	7700	4.000	22.5	92	33	–	–	–	7	1	3.445	2.564
95	102598868	7750	3.900	35.0	76	26	6	2	3.003	10,8	2,2	2.462,3.294	2.564
96	102599598	7600	4.000	65.0	99	55	22,19	5,4	2.429,3.387	42,37	9,7	2.584,1.835	1.552

NOTE. — Columns: (1) the running number (No.), (2) the CoRoT ID, (3) the effective temperature ($T_{\rm eff}$), (4) the surface gravity ($\log g$), (5) the radial velocity ($v_{\rm rad}$), (6) the number of SigSpec frequencies (SSF), (7) the number of filtered frequencies (FF), (8) the number of frequencies included in the sequences from the VI (EF$_{\rm VI}$), (9) the number of sequences from the VI (SN$_{\rm VI}$), (10) the dominant spacing from the VI (SP$_{\rm VI}$), (11) the number of frequencies included in the sequences from the SSA (EF$_{\rm A}$), (12) the number of sequences from the SSA (SN$_{\rm A}$), (13) the dominant spacing from the SSA (SP$_{\rm A}$), (14) the spacing from the FT (SP$_{\rm FT}$).

The SSA scans through the frequency lists and selects frequency sequences defined by Eq. (1) with a parameter set D, Δf and n. The search begins from the highest amplitude frequency f_1 that we called *basis frequency*. The search proceeds with the frequency $\hat{f}_1$ the closest neighbor of f_1, if $|\hat{f}_1 - f_1| \leq D$ and $|\hat{f}_1 - f_1| > \Delta f$. If the $\hat{f}_1$ is too close (viz. $|\hat{f}_1 - f_1| \leq \Delta f$), the algorithm steps to the next frequency $\hat{f}_2$ and so on. We collect the sequences $S_1, S_2, \ldots, S_N, (N \leq i)$ found by the search from the frequencies $f_1, \hat{f}_1, \hat{f}_2, \ldots, \hat{f}_{i-1}$ as a *pattern* belonging to a given D and basis frequency f_1. Next, the algorithm goes to the second highest-amplitude frequency f_2 and (if it is not the element of the previous pattern) begins to collect a new pattern again. On the basis of the VI (Sec. 3.1) we demanded that at least one of the two highest amplitude frequencies must be in a pattern, so we did not search from smaller amplitude frequencies ($f_i, i \geq 3$) as a basis frequency.

Starting from the parameter range obtained by the VI we made numerical experiments determining the optimal input parameters. We found the smallest difference between the results of the automatic and visual sequence search at $\Delta f = 0.1$ d^{-1}. Since we do not have any other reference point, we fixed Δf at the this value. If we chose n (the length of the sequence) to be small ($n \leq 3$) we ob-

tained a huge number of short sequences for most of the stars. Avoiding this, we set $n = 4$. The crucial parameter of the algorithm is the spacing D. Our program determines D in parallel with the sequences. The primary searching interval was $D_{\rm min} = 1.5 \leq D \leq 7.8 = D_{\rm max}$. The lower limit was fixed according to our results obtained by the VI. To reduce the computation time we applied an adaptive grid instead of an equidistant one. We calculated the spacings between the ten highest amplitude frequencies for each star $D_{1,2} = |f_1 - f_2|$, $D_{1,3} = |f_1 - f_3|$, ..., $D_{9,10} = |f_9 - f_{10}|$. The $D_{l,m}$ values could be either too high or too low for a large separation, therefore we selected those ones where $D_{\rm min} \leq D_{l,m} \leq D_{\rm max}$ and restricted our further investigations to this selected $D_{l,m}$. Then we define a fine grid around all such spacings with $D_{l,m,h} = D_{l,m} \pm h\delta f$, where $h = 15$ and $\delta f = 0.01$ d^{-1}. The SSA script ran for all $D = D_{l,m,h}$ searching for possible sequences for all D values.

The SSA script calculates (1) the total number of frequencies in all series for a given D, which is the frequency number of the pattern, (2) the number of found sequences, (3) the actual standard deviation of the echelle ridges and (4) the amplitude sum of the pattern frequencies. These four output values helped us to recognize the dominant spacing, since the algorithm revealed in many stars two or three characteristic spacings. The similar parameters that we derived by VI, the number of the frequencies in the sequences (EF$_{\rm A}$), the number of sequences (SN$_{\rm A}$) and the spacings (SP$_{\rm A}$) are given in the 11th, 12th and 13th column of Table 3. The algorithmic search recognized many more spacing values. Obviously, when we have more spacings, the appropriate set of frequencies and the number of frequencies are also given. The best solutions are given at the first place of the columns.

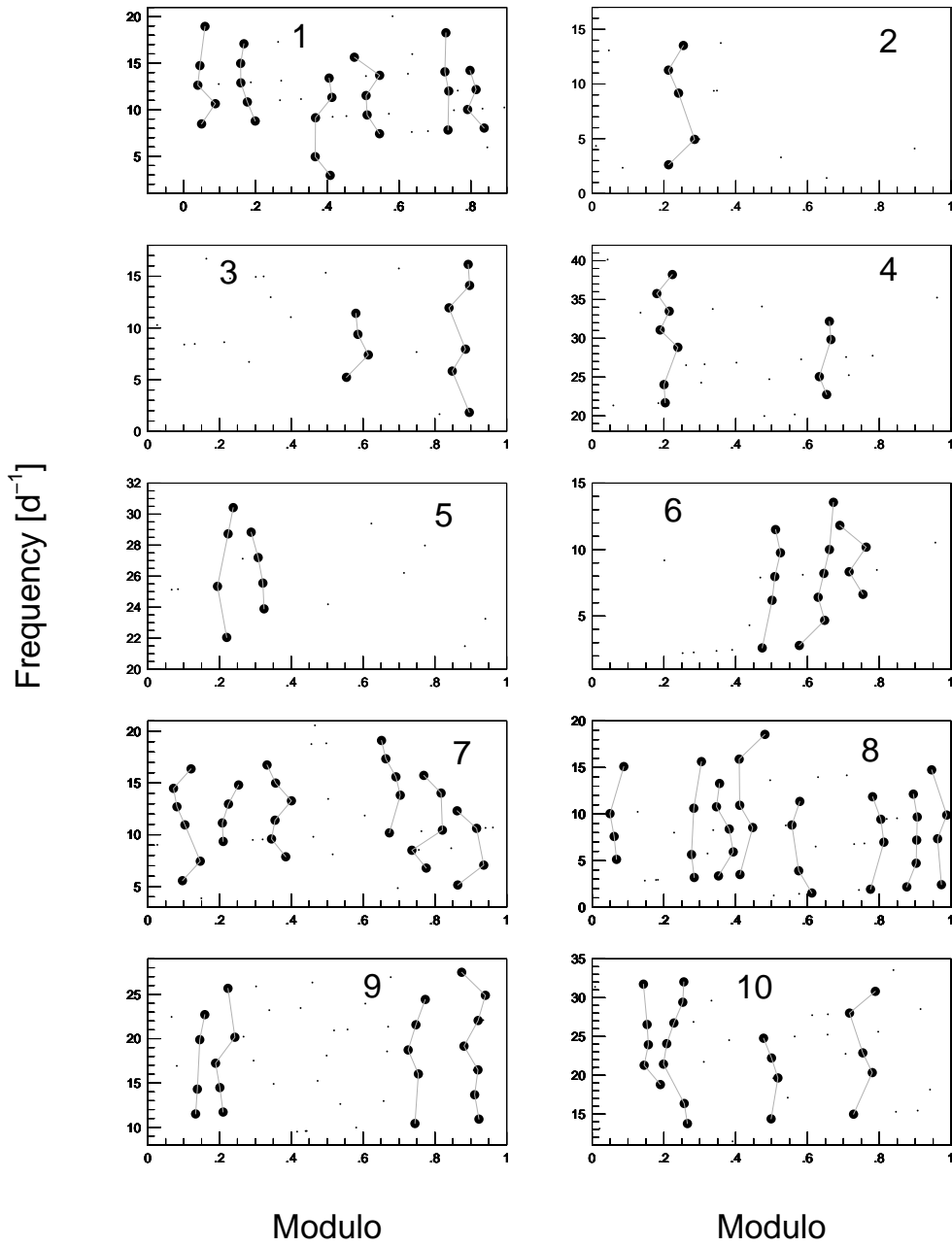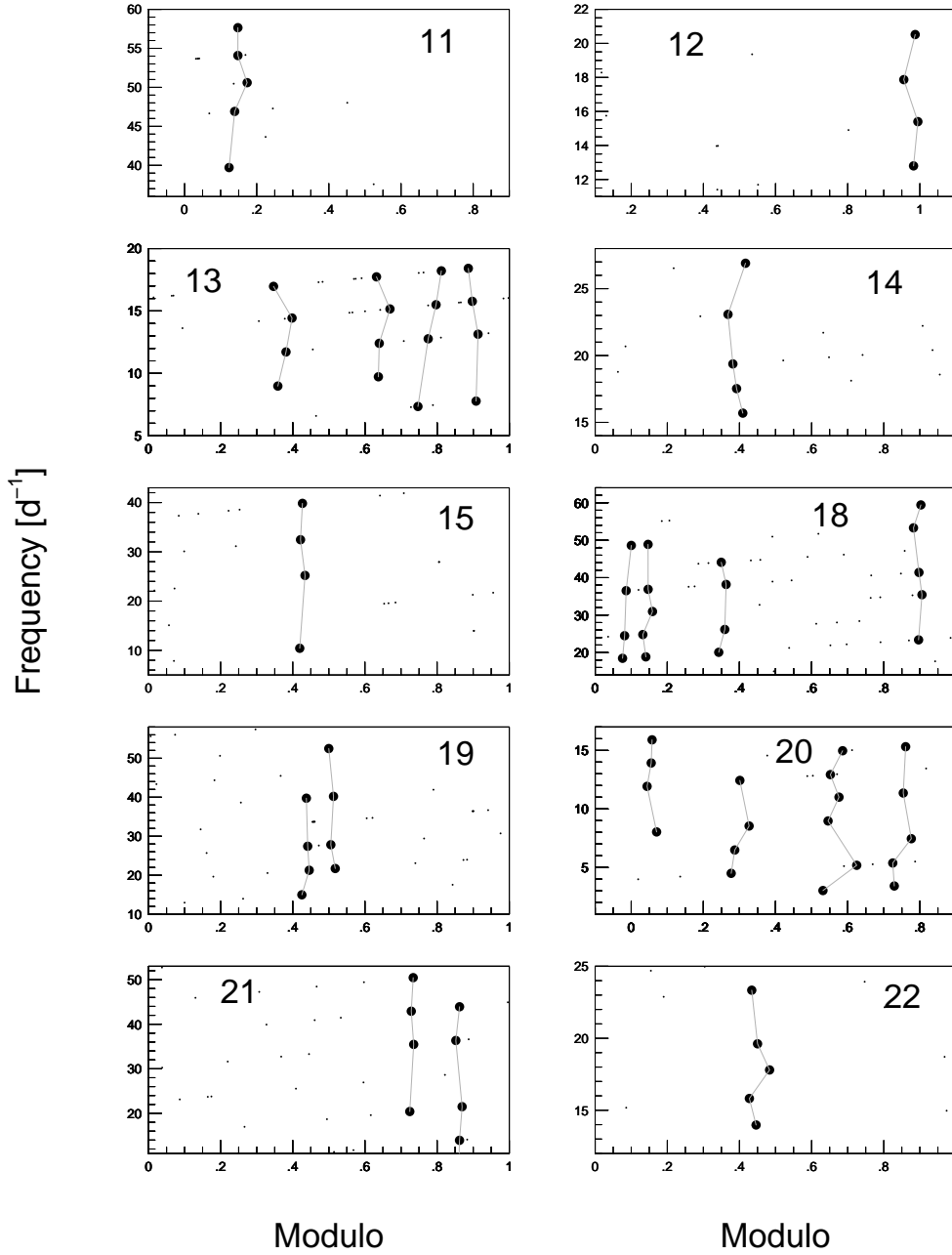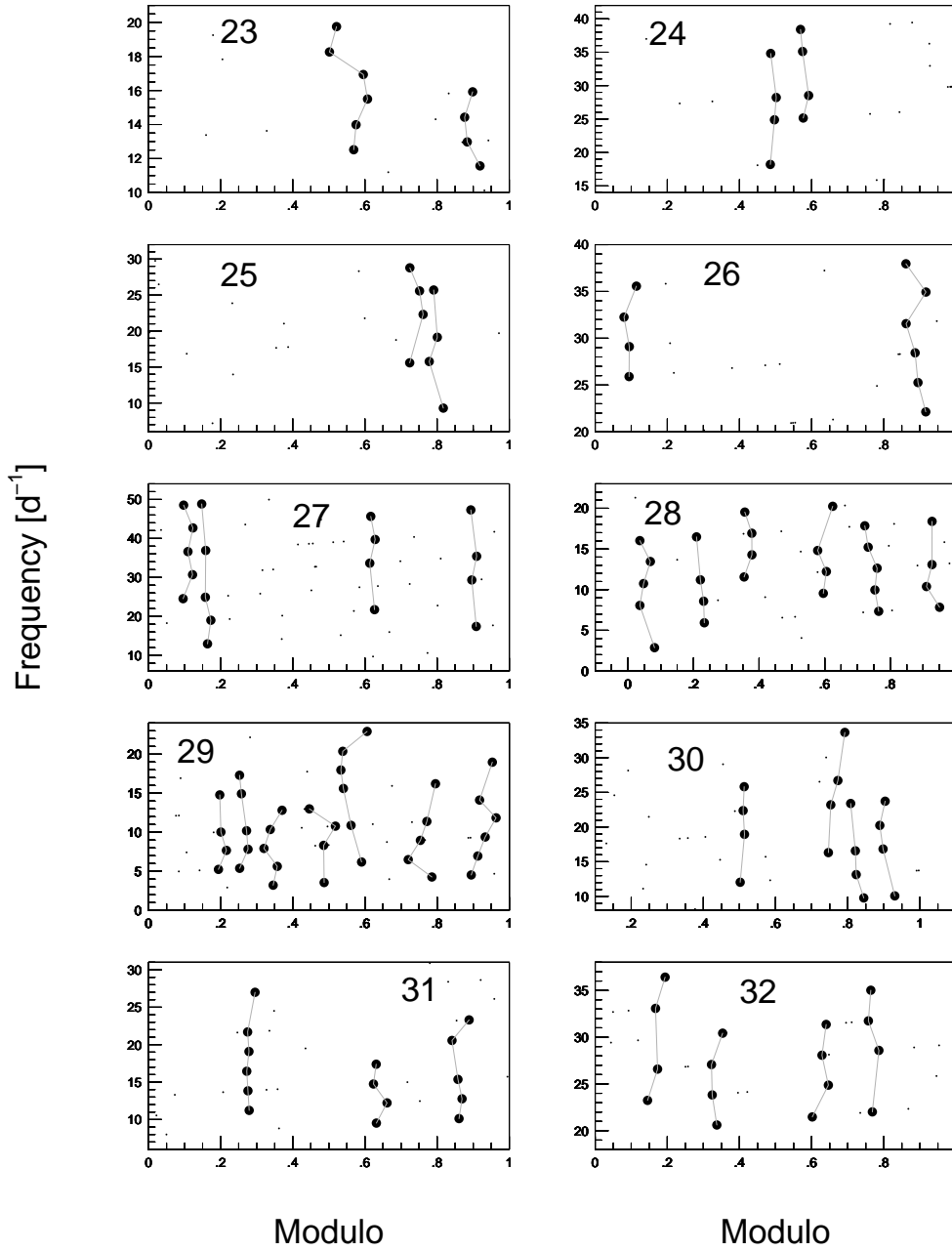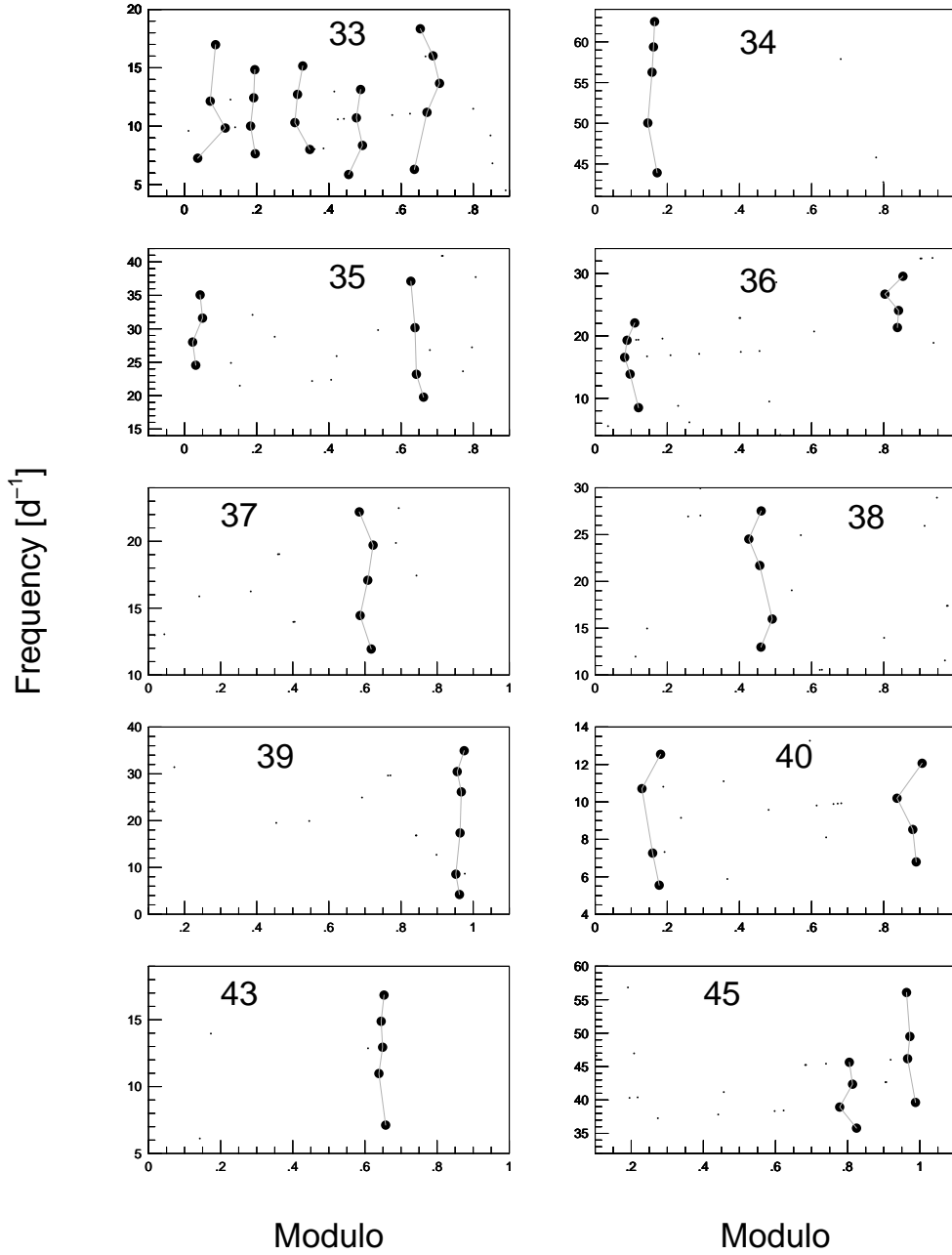The sequences obtained by SSA are also flagged in the

Fig. 3.— Echelle diagrams using the best spacing obtained by SSA. The labels mark the running number of stars in our sample. The spacings used for modulo calculation are 2.092, 2.161, 2.046, 2.356, 1.668, 1.767, 1.795, 2.481, 2.784, and 2.614 d^{-1} for the increasing running numbers, respectively.
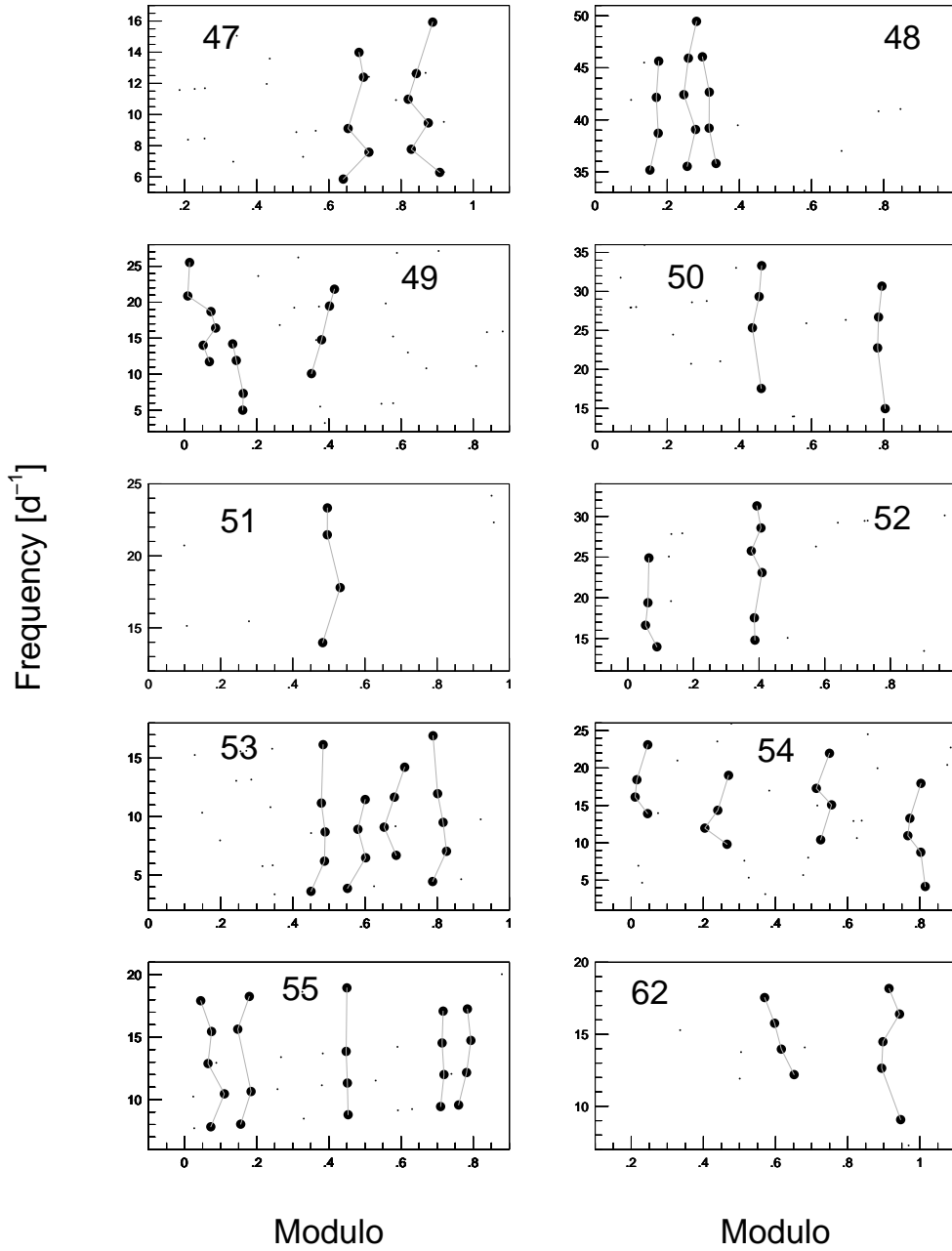
FIG. 4.— Echelle diagrams using the best spacing obtained by SSA. The labels mark the running number of stars in our sample. The spacings used for modulo calculation are 3.570, 2.569, 2.674, 1.866, 7.342, 6.001, 6.175, 1.478, 7.492, and 1.877 d^{-1} for the increasing running numbers, respectively.
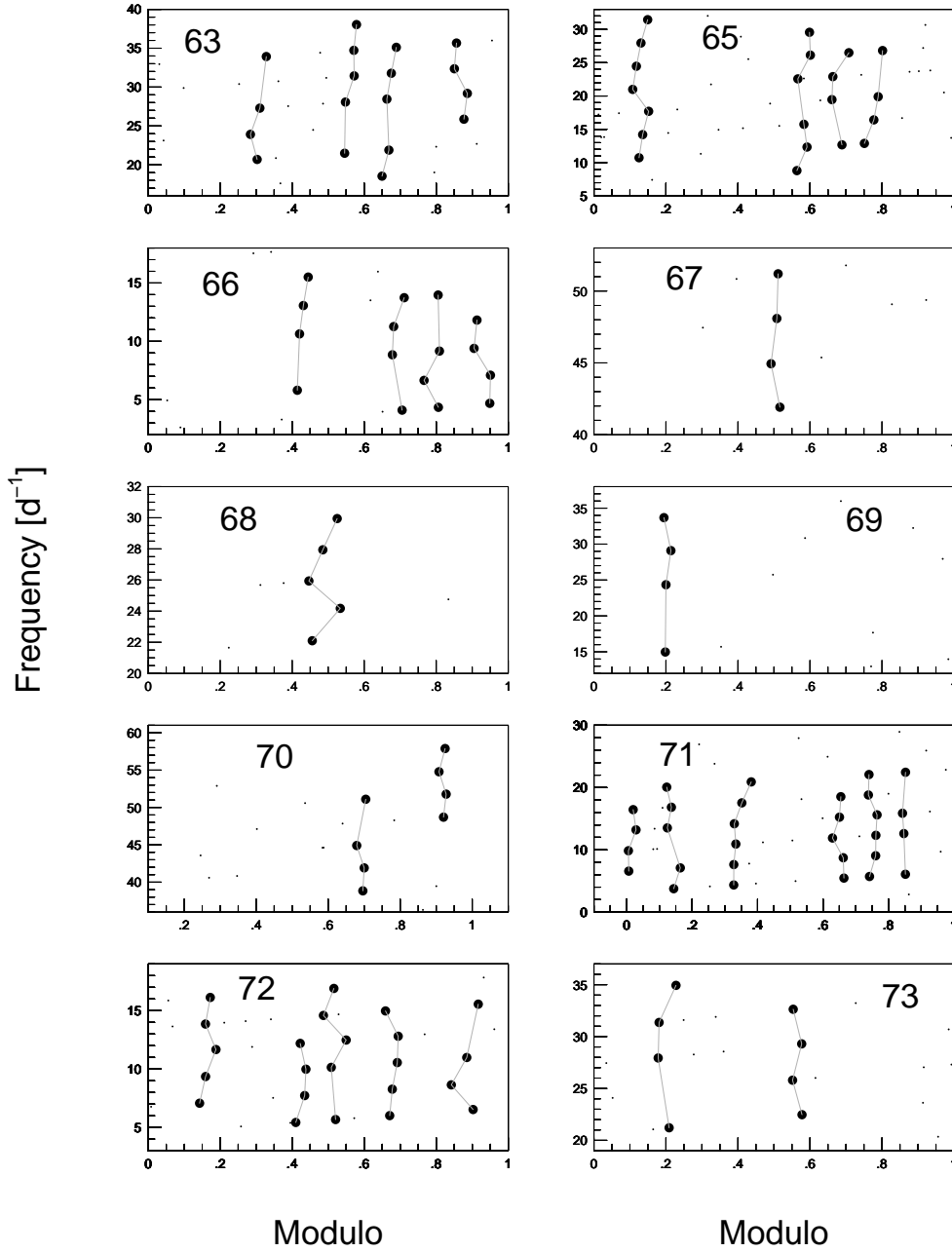
FIG. 5.— Echelle diagrams using the best spacing obtained by SSA. The labels mark the running number of stars in our sample. The spacings used for modulo calculation are 1.461, 3.320, 3.299, 3.200, 5.995, 2.655, 2.389, 3.082, 2.622, and 1.671 d^{-1} for the increasing running numbers, respectively.

FIG. 6.— Echelle diagrams using the best spacing obtained by SSA. The labels mark the running number of stars in our sample. The spacings used for modulo calculation are 2.396, 3.099, 3.492, 2.723, 2.586, 2.910, 4.382, 1.747, 1.947, and 3.306 d^{-1} for the increasing running numbers, respectively.
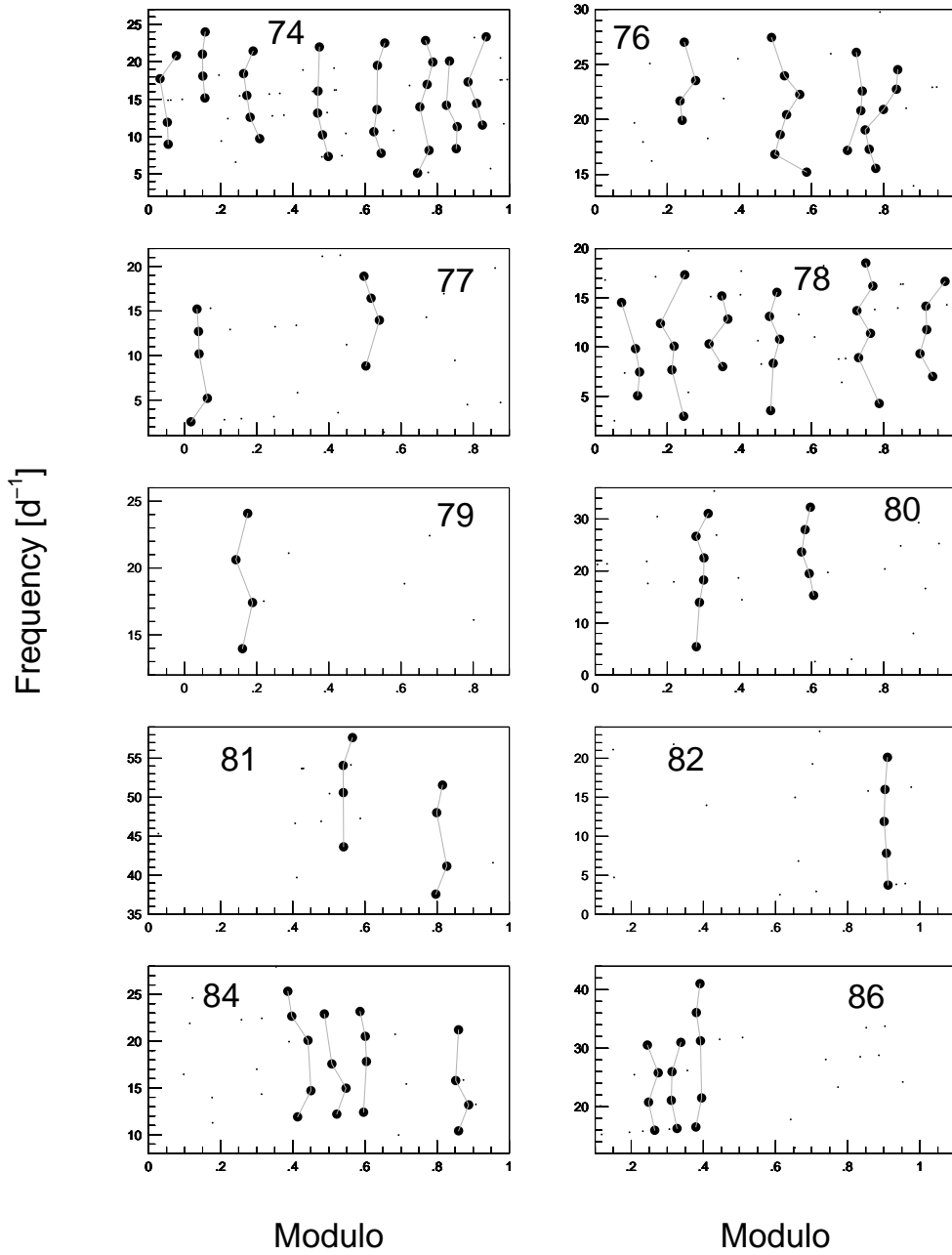
Paparó et al.

FIG. 7.— Echelle diagrams using the best spacing obtained by SSA. The labels mark the running number of stars in our sample. The spacings used for modulo calculation are 1.611, 3.464, 2.317, 3.936, 1.867, 2.748, 2.492, 2.300, 2.544, and 1.834 d^{-1} for the increasing running numbers, respectively.

FIG. 8.— Echelle diagrams using the best spacing obtained by SSA. The labels mark the running number of stars in our sample. The spacings used for modulo calculation are 3.285, 3.437, 2.406, 3.101, 1.929, 4.682, 3.059, 3.495, 2.249, and 3.416 d^{-1} for the increasing running numbers, respectively.
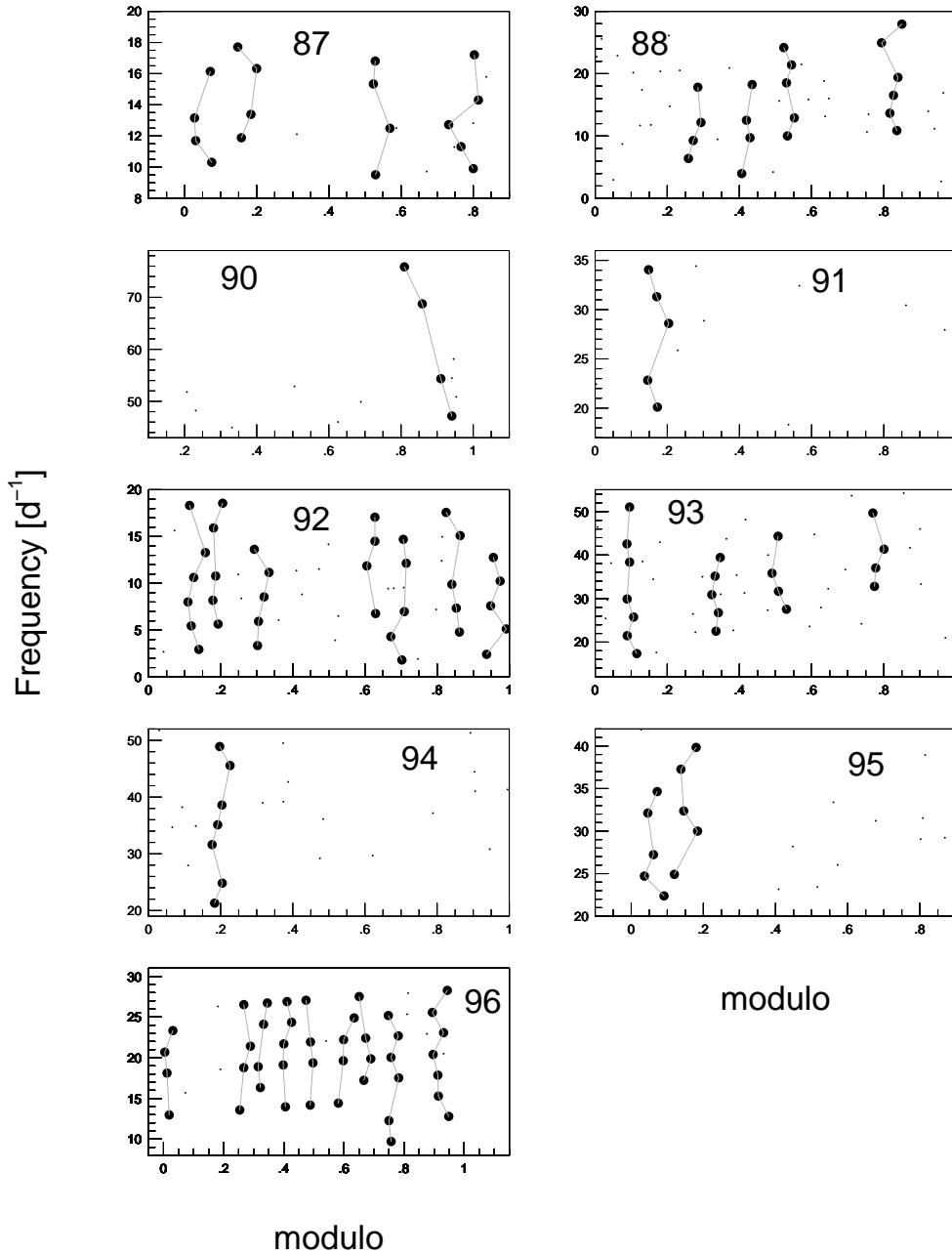
FIG. 9.— Echelle diagrams using the best spacing obtained by SSA. The labels mark the running number of stars in our sample. The spacings used for modulo calculation are 2.940, 1.772, 2.521, 2.392, 3.357, 4.247, 3.480, 4.098, 2.699, and 4.890 d^{-1} for the increasing running numbers, respectively.

FIG. 10.— Echelle diagrams using the best spacing obtained by SSA. The labels mark the running number of stars in our sample. The spacings used for modulo calculation are 1.862, 2.837, 7.170, 2.803, 2.576, 4.219, 3.445, 2.462, and 2.464 d^{-1} for the increasing running numbers, respectively.

electronic table in additional columns (see in Table 2). SSA1, SSA2..., etc. agree with the first, second,..., etc. value of the spacing. The flags are similar as in the case of VI (0 – not included, 1, 2, 3, . . ., are the frequencies of the 1st, 2nd, 3rd, . . ., sequences).

The summary of the results on SSA is the following. SSA found independent solutions for 73 stars. Unexpectedly, the test cases showed seemingly more diversity. As we noticed from the beginning, the filtering process resulted, for some cases, in quite different number of frequencies used in the SSA. Comparing to the number of the SigSpec frequencies, the differences in the resulted frequency content of the double-checked stars is not remarkable, in most cases less than 10%. In any case there are block of frequencies of highest amplitudes that are common to both files of the double checked cases. This guarantees that the SSA uses the same basis frequencies for the sequence search. Keeping the differences of the frequency content of the double-checked cases, we intended to check the sensitivity of the SSA to the frequency content. It is obvious that if we have a larger frequency content, then we find more sequences and more frequencies located on the echelle ridges. Of course, this will also influence the mean spacings. Nevertheless, as Table 3 shows, the spacings differ by less than 10%.

The comparison of the two approaches, VI and the SSA gives the following result. They resulted in similar spacing for 42 stars. In the SSA we found six cases with half of the VI values. In 23 cases different spacing values were found. The seemingly large number contains the cases where we did not find any sequences in the star by one of the two approaches (12 for VI and 4 for SSA. There is no overlap in these subsets).

The best spacings found by the algorithm for the CoRoT targets (the first value of 13th column) are used to create the echelle diagrams presented in Figs. 3-10. All filtered frequencies are plotted (small and large dots), while the frequencies located on an echelle ridge are marked by large dots. Taking into account the fixed ± 0.1 d^{-1} tolerance we may not expect to find any effects caused by the change in chemical composition (glitches) or effects caused by the evolution (avoided crossing). However, we may conclude that we found unexpectedly large numbers of regular frequency spacing in our sample of CoRoT δ Scuti stars. Any relation that we find among the echelle ridges, the physical parameters and the estimated rotational splitting confirms that the echelle ridges are not an accidental arrangement of unrelated frequencies along an echelle ridge.

3.3. *Fourier Transform (FT)*

Fourier Transform (FT) of the frequencies involved in the pulsation is, nowadays, widely used in searching period spacing and finding the large separation since Handler et al. (1997) to García Hernández et al. (2015). It is worthwhile to compare the spacing obtained by FT and by our sequence search method. We followed the way described by Handler et al. (1997) (instead of the way introduced by Moya et al. 2010) and derived the FT spacing (the highest peak) for our sample, given in the 14th column of Table 3.

The FT of the star No. 65 is shown in Fig. 11. The highest peak suggests a large separation at 1.282 d^{-1} that does not agree with the spacing obtained by the
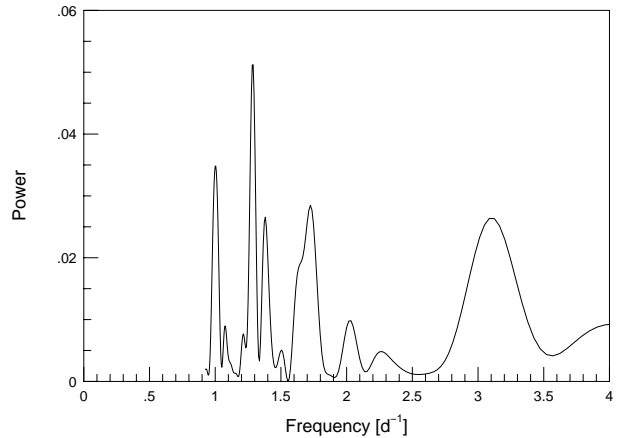

Fig. 11.— Fourier Transform of star No. 65. The highest peak at 1.282 d^{-1} agrees with a shift of sequences in VI. The lower amplitude peak agrees with 3.459 or 3.437 d^{-1} spacings that are obtained by VI and SSA, respectively.
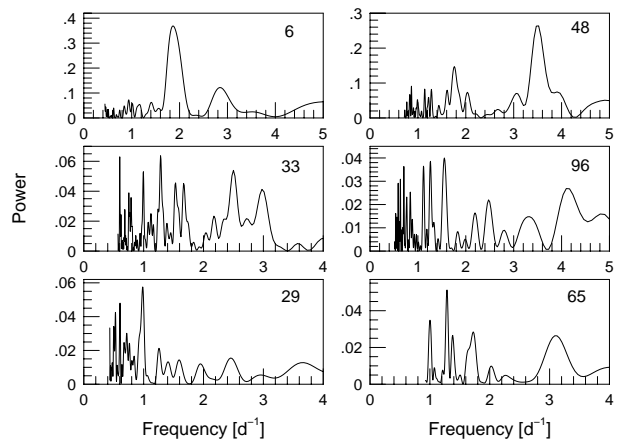

Fig. 12.— Some characteristic examples of FT in our sample. The labels mark the running number of the star. The simplest and the most complex examples are in the top and the middle panels. The bottom panels show examples with very low value of the spacing. Both VI and SSA resulted in higher values. The highest peak probably represents a shift between sequences.

VI and SSA (3.459 and 3.437 d^{-1}, respectively). FT spacing is closer to the characteristic shifts derived for the third sequence relative to the first one (1.209 d^{-1}) to the leftward direction. The FT shows a peak near our value but it is definitely not the highest peak.

A general comparison of FT spacing to our spacing values, both visual (VI) and algorithmic (SSA), reveals that the two methods (three approaches) do not yield a unique solution. There are cases when VI, SSA and FT spacings are the same (stars No. 2, 4, 5, 6, 11, 48 and 79) despite the spacings being around 2.2±0.1 d^{-1} (stars No. 2 and 4) or around 1.7±0.2 d^{-1} (stars No. 5 and 6) or around 3.5±0.1 d^{-1} (stars No. 11, 48 and 79). As the echelle diagrams show, these stars have the simplest regular structure. There are cases when VI and SSA
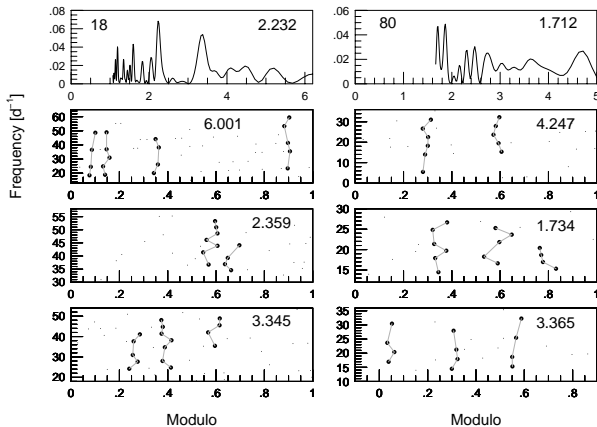
FIG. 13.— Comparison of FT diagram and echelle diagrams with three different spacings obtained by SSA for stars No. 18 and 80. The top panels give the FT diagram. These panels are marked by the highest peak. The other panels are marked by the spacing used for getting the echelle diagrams. The highest peak of FT and the best solution of SSA do not agree.

TABLE 4
SPACING DISTRIBUTIONS

Range	N_{VI}	N_{SSA}	N_{FT}
0-1	—	—	7
1-2	5	16	25
(1-1.5	—	2	13)
(1.5-2	5	14	12)
2-3	35	31	23
3-4	26	19	16
4-5	3	6	9
6-7	1	3	3
7-	—	3	—

NOTE. — Distribution of spacings obtained by different methods in 1 d^{-1} bins. The columns show the spacing range and the number of the spacings found by the methods VI, SSA, and FT within the given range.

spacings are the same (stars No. 8, 12, 25 and 43), but the FT shows different spacings. There are cases, when VI and FT spacings are the same (stars No. 19 and 24) or SSA and FT spacings are the same (stars No. 13, 23, 32 and 39). In Fig. 12 we present some characteristic examples of FT, representing the simplest cases (upper panels), the most complicated cases, when the decision which is the highest peak is hard (middle panels), and cases when FT shows a completely different spacing than VI and SSA (bottom panels). Our example for the visual inspection, star No 65, belongs to this group. We omitted the low-frequency region applying the Nyquist frequency to the FT.

We present the numbers of the spacings in 1 d^{-1} bins for the different methods in Table 4. The numbers in a bin are slightly different for VI and SSA, but FT shows a remarkably higher number in the 0-1 and 1-2 d^{-1} region of the spacings. In a latter phase the 1-2 d^{-1} bin was divided in to two parts to avoid the artifact of the lower limit of SSA for spacing (1.5 d^{-1}). VI and SSA have low numbers in the 1-1.5 d^{-1} bin, while FT has much higher value. The VI definitely interpreted such a spacing as a shift of the sequences. SSA has lower value probably due to the lower limit that we learned from the VI. In the 1.5-2.0 d^{-1} bin the VI still has lower population but SSA and FT found a similar population. In both cases there is no additional search for the shifts of the sequences.

It is worthwhile to see how the different SSA spacings, when more are obtained, are related to the FT spacing. We present two cases. The FT diagram and the echelle ridges where we used the different spacings are shown in Fig. 13. Left panels belong to star No. 18, while right panels to star No. 80. The panels are labeled with the actual spacing value that we used for the calculation of the modulo values. The top panels show the FT. The second panels give the dominant SSA spacing resulting in the most straight echelle ridges, but the other values also fulfill the requirement of SSA. The FT agrees with one of the SSA spacings, but not necessarily with the

dominant SSA spacing.

We conclude that the different methods (with different requirements) are able to catch different regularities among the frequencies. The different spacing values are not a mistake of any method but the methods are sensitive to different regularities. The VI and SSA concentrate on the continuous sequence(s), while the FT is sensitive to the number of similar frequency differences, disregarding how many sequences are among the frequencies. When we have a second sequence with a midway shift, then the FT shows it, instead of the spacing of a single sequence. The spacing of a single sequence will be double the value of the highest peak in FT.

If the shifts of the sequences are asymmetric, the FT shows a low and a larger value with equal probability. When we have many peaks in the FT, then it reflects that we have many echelle ridges with different shifts with respect to each other. The sequence method helps to explain the fine structure of the FT.

4. TEST FOR REFUSING ARTIFACTS AND CONFIRMATION OF SEQUENCES

The comparison of spacing obtained by three different approaches results in a satisfactory agreement if we consider the different requirements. However, the spacing is the only point where we are able to compare them, since this is the only output of FT. We cannot compare the unexpectedly large number of echelle ridges (sequences), since we identified them for the first time. What we can do and what we really did, is to make any test that can rule out some possible artifacts and confirm the existence of so many sequences with almost equal spacing in δ Scuti stars.

(1) We started with a very basic test. Can we get the echelle ridges as a play of randomness on normally distributed frequencies? Three tests, one-dimensional Kolmogorov-Smirnov (K-S) test, Cramér-von Mieses test, and the χ^2-test were applied to our frequency list for the stars and to randomly generated frequency lists. The frequency distribution of 14 stars showed significant differences from the normal distribution, but in the mathematical sense most of our frequency list proved to be randomly distributed. The surprising mathematical test inspired more check.

The classical K-S test and its more sensitive refine-

ments such as Anderson-Darling or Cramér-von Mieses tests are successfully applied for small samples. These tests are indeed the suggested tools for small element (~ 20) samples. Our frequency lists have 9-68 elements; the average value is 32.8. We prepared a 30-element equidistantly distributed artificial frequency list. In our phrasing all the 30 frequencies build one single sequence. None of the tests, however, found significant differences from the randomness. If we increase the number of our synthetic data points and we reach 100-200 elements (depending on the used test) the tests detect the structure, viz. the significant (95%) difference from the normal distribution.

As an additional control case, we tested 30 frequencies of a pulsating model of FG Vir (discussed in paper Part I). All tests revealed that the model frequencies (l=0, 1, and 2) were also randomly distributed, although these frequencies were a result of a pulsation code and a sequence of grouped frequencies was reported for FG Vir (Breger et al. 2005). Adding the rotational triplets and multiplets (64 frequencies) to the list (altogether 94 frequencies), the tests proved a significant difference from the normal distribution. We conclude that these statistical tests would give correct results for our specific distributions only if we had two to four times more data points than we have. The present negative results have no meaning; they are only small sample effects. In other words, such global statistical tests are not suitable tools for detecting or rejecting any structures in our frequency lists.

(2) If the echelle ridges that we found were coincidences only, we could find similar regularities for random frequency distribution as well. Checking this hypothesis we have chosen three stars which represent well our results: the stars No. 39, 10 and 92 show a single sequence with 6 frequencies, four sequences with 21 frequencies (the average length of a sequence is 5.25), and 7 sequences with 35 frequencies (average length = 5), respectively. We prepared 100 artificial data sets for each of these stars. The data sets contain random numbers as frequencies within the interval of the real frequency intervals. The number of the random "frequencies" is the same as the number of the real frequencies. The real star amplitudes are randomly assigned to the synthetic frequencies. We run the SSA on these synthetic data with the same parameters as we used for real data. We found the following results.

We compared two parameters of the test and real data: the total number of frequencies located on echelle ridges, and the average length of the sequences. In the most complex case (star No. 92) we did not find a regular structure in the simulated data, for which the total number of frequencies located on the echelle ridges is as high as in the real star (35). In the two simpler cases only 5% (for star No. 39) and 2% (for star No. 10) of the echelle ridges proved to be as long as in the real stars.

These Monte Carlo tests show that the coincidence as an origin of few of the echelle ridges that we found in our sample stars cannot be ruled out completely, but the probability of such a scenario is low ($<5\%$) and depends highly on the complexity of the echelle ridges (the more echelle ridges the lower the probability). This could concern, in the case of our sample, a maximum of one to three stars.

(3) Obviously a basic test was whether any regularity can be caused by the instrumental effects (after removing most of them) and whether data sampling resulted in the systematic spacing of the frequencies? The well-known effect from the ground-based observations (especially from single sites) is the 1, 2, ..., d^{-1} alias structure around the pulsation frequencies. In this case, we worked on continuous observation with the CoRoT space telescope. In principle, it excludes the problem of alias structure, but the continuity is interrupted from time to time by the non-equal long gaps caused by passing through the South Atlantic Anomaly (SAA). In the spectral window pattern the only noticeable alias peak is at 2.006 d^{-1} and sometimes an even lower peak around 4 d^{-1}. The expected alias structure around any pulsation peak is only 2 percent. A test on a synthetic light curve was presented by Benkő & Paparó (2015). Comparison of the equally spaced and gapped data shows no difference in the frequencies. The requirement for a sequence containing four members is, at least, a quintuplet structure of the alias peaks around the frequencies of the highest amplitude, which is very improbable for the CoRoT data. We may conclude that our sequences are not caused by any alias structure of the CoRoT data. Table 3 contains some spacings with near integer value, but in most cases different methods yielded different values. In an alias sequence we must have strictly equal spacing and mostly only one echelle ridge.

(4) The linear combination of the higher amplitude modes creates a systematic arrangement of the frequencies reflecting the spacing between the highest amplitude modes. A high amplitude δ Scuti star, CoRoT 101155310 (Poretti et al. 2011) was used as a control case for two reasons. No systematic spacing was found for the 13 independent frequencies by our SSA algorithm which means the star does not show any instrumental effects discussed in the previous paragraph. To complete the list with the linear combination, our algorithm found a dominant spacing around 2.67 d^{-1} which is near the frequency difference of the highest amplitude modes.

Our visual inspection and algorithmic search were based on the investigation of the spacing of the peaks of the highest amplitude. It was necessary to check the frequency list for linear combinations. Half of our targets (44) showed linear combinations, with one (15) or two (12) $f_a + f_b = f_c$ connections. In some cases (stars No. 21, 54, 66, 78, 7, 74 and 8) 9-14 linear combination frequencies were found. Comparing these to the frequencies in the echelle ridges, we found that the linear combinations were not included in the echelle ridges. There is only a single case (star No. 71.) where the echelle ridge at around 0.18 modulo value contains three members of a linear combination. In other cases, only two members fit the echelle diagrams. Star No. 38 is a critical case, where by omitting a member of the linear combination frequencies, we have to delete the single echelle ridge. We conclude that the echelle structure is not seriously modified in the other targets.

All echelle frequencies connected to linear combinations in our stars were compared. The frequencies are different from star to star, so the connection between the frequencies does not have any technical origin.

(5) To keep the human brain's well-known property in check, namely that it searches everywhere for struc-

TABLE 5
Comparison of spacings

Star	SP_p (d^{-1})	SP_A (d^{-1})	EF_A	SN_A
44 Tau	2.25	4.62	22	5
BL Cam	7.074	7.11	8	2
FG Vir	3.7	3.86	15	3
KIC 8054146	2.763	2.82,3.45	7,12	1,2

Note. — The first two columns contain the star name and published spacing SP_p. The last three columns show the results of our SSA search: spacing (SP_A), the total number of frequencies in all sequences (EF_A), and the number of found sequences (SN_A), respectively.
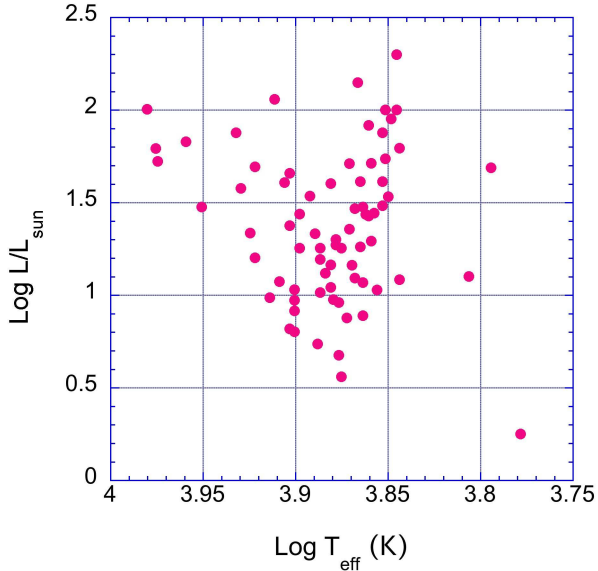

Fig. 14.— Theoretical HR diagram derived from the parameters obtained from the AAO spectroscopy. The location of the targets was used to derive the estimated rotational velocity and rotational frequencies

tures (visual inspection) or any artifact in the algorithm, we used well-known δ Scuti stars as test cases. Spacing of consecutive radial orders were published for different δ Scuti stars: 44 Tau (Breger & Lenz 2008), BL Cam (Rodríguez et al. 2007), FG Vir (Breger et al. 2005), summarized by Breger et al. (2009) and KIC 8054146 (Breger et al. 2012). We checked these stars by our SSA algorithm to see whether we would find similar results or not.

We summarize the results in Table 5. The published and the SSA spacings are in good agreement (2nd and 3rd columns). For 44 Tau we found double the value of the published spacing. In the case of KIC 8054146 we found a second spacing by SSA in addition to the first matching spacing. We also present the number of frequencies involved in the sequences and the number of sequences (4th and 5th columns).

We conclude that our algorithm finds the proper spacing of the data and the VI does not simply reflect the human brain. We confirmed that the echelle ridges belong to the pulsating stars and reflect the regularities connected to the stars.

5. ROTATION-PULSATION CONNECTION

The basic problem of the mode identification in δ Scuti stars is partly the lack of regular arrangement of the frequencies predicted by the theory. Further complication is caused by the rotational splitting of the non-radial modes, especially for fast rotating stars. Application of our sequence search method for δ Scuti stars revealed an unexpectedly large number of echelle ridges in many targets. Knowing the regular spacing of the frequencies we wonder whether we can find a connection between the echelle ridges and the rotational frequency of the stars.

5.1. Estimated rotational velocities

We do not have rotational velocity independently measured for our targets. Nowadays the space missions have enormously increased the number of stars investigated photometrically with extreme high precision, but the ground-based spectroscopy cannot keep up with this increase. However, for our targets we have at least AAO spectroscopy for classification purposes (Guenther et al. 2012; Sebastian et al. 2012).

Based on the AAO spectroscopy one of us (Hareter 2013) derived the T_{eff} and $\log g$ values for our sample used the same rotational velocity ($100~km^{-1}$) for all the stars (see Table 3). The error bars are also given in Hareter (2013). For giving insight to the error of AAO spectroscopy we present the most typical range of errors for T_{eff} and $\log g$. For 70% of the stars the error of T_{eff} falls in the range of 50-200 K. In a few cases (≤ 9) the errors are over 1000 K. For $\log g$ the typical range is 0.2-0.8, that represents of the 83% of the stars. The physical parameters were used to plot our targets on the theoretical HR diagram as shown in Fig. 14. To get a more sophisticated knowledge on the rotation of our targets we followed the process of Balona et al. (2015) who determined 10 boxes on the theoretical HR diagram. Using the catalog of projected rotational velocities (Glebocki & Stawikowski 2000) they determined the distribution of $v \sin i$ for each box. The true distribution of equatorial velocities in the boxes was derived by a polynomial approximation (Balona 1975). Using the characteristic equatorial rotational velocities of the boxes we derived the estimated equatorial rotational velocity and the rotational frequency for each target presented in Table 6. To obtain the rotational frequency, an estimate of the stellar radius is required; we followed Balona et al. (2015) in using the polynomial fit of Torres et al. (2010) developed from studies of 94 detached eclipsing binary systems plus α Cen. The polynomial fit is a function of T_{eff}, $\log g$, and [Fe/H]; we assume solar metallicity for our estimates. The radii calculated this way are also given in Table 6. We also included the mass and the mean density in the table, calculating these using the Torres et al. (2010) polynomial fit for mass and radius.

Although these are only estimated values, they allow us to compare the rotational frequency and the shifts between the sequences to search for a connection between them, if there is any.

5.2. Echelle ridges and rotation

We have three parameters that we can compare for our targets, namely the shift of the sequences, the rotational frequencies derived, and the spacing, or in some cases the

TABLE 6
Estimated sterllar properties

Star	R ($R_\odot$)	V_{eq} (km s^{-1})	Ω_{rot} (d^{-1})	M ($M_\odot$)	ρ (g cm^{-3})	Star	R ($R_\odot$)	V_{eq} (km s^{-1})	Ω_{rot} (d^{-1})	M ($M_\odot$)	ρ (g cm^{-3})
1=55	3.911	80	0.404	2.046	0.0482	49	1.936	130	1.327	1.725	0.3349
2=66	3.985	110	0.545	2.528	0.0563	50	2.176	110	0.999	1.728	0.2360
3	9.641	80	0.164	3.044	0.0048	51	3.414	80	0.463	1.976	0.0699
4	2.340	70	0.591	1.776	0.1952	52	1.745	130	1.472	1.764	0.4681
5	2.409	70	0.574	1.677	0.1690	53	5.402	110	0.402	2.726	0.0244
6	3.335	140	0.829	2.527	0.0959	54	5.797	100	0.341	2.486	0.0180
7	6.370	80	0.248	2.519	0.0137	55=1	3.911	80	0.404	2.046	0.0482
8=92	3.540	110	0.614	2.248	0.0714	56	3.347	110	0.649	2.013	0.0756
9	5.726	100	0.345	2.428	0.0182	62	2.311	150	1.282	2.184	0.2492
10	2.679	110	0.811	1.840	0.1348	63	3.448	110	0.630	2.014	0.0692
11=81	1.347	130	1.907	1.660	0.9574	65	4.008	100	0.493	2.146	0.0470
12	1.928	150	1.537	1.920	0.3770	66=2	3.985	110	0.545	2.528	0.0563
13=74	6.651	100	0.297	2.588	0.0124	67	1.767	130	1.454	1.809	0.4620
14=96	2.222	130	1.156	1.800	0.2309	68	3.304	140	0.837	2.204	0.0860
15	1.352	130	1.899	1.674	0.9532	69	1.297	90	1.371	1.541	0.9955
18	1.143	90	1.555	1.499	1.4126	70	1.633	130	1.573	1.734	0.5611
19	1.796	90	0.990	1.669	0.4055	71	3.702	140	0.747	2.767	0.0768
20	2.986	110	0.728	3.073	0.1626	72	7.355	100	0.269	2.812	0.0100
21	1.825	130	1.407	1.721	0.3988	73	2.406	130	1.068	1.875	0.1897
22	1.248	40	0.633	1.153	0.8345	74=13	6.651	100	0.297	2.588	0.0124
23	6.039	80	0.262	2.151	0.0138	75	2.913	40	0.271	1.629	0.0929
24	2.282	110	0.952	1.897	0.2247	76	2.907	110	0.748	1.923	0.1103
25	2.220	150	1.335	2.015	0.2595	77	4.235	80	0.373	2.131	0.0395
26	2.547	150	1.163	1.870	0.1593	78	4.910	70	0.282	2.260	0.0269
27	1.668	130	1.540	1.616	0.4903	79	2.161	70	0.640	1.704	0.2378
28	5.430	80	0.291	2.318	0.0204	80	3.347	110	0.649	2.013	0.0756
29	2.096	110	1.037	3.232	0.4947	81=11	1.347	130	1.907	1.660	0.9574
30	3.649	80	0.433	2.005	0.0581	82	1.320	130	1.945	1.596	0.9770
31	2.135	70	0.648	1.664	0.2409	83	2.558	140	1.081	1.997	0.1680
32	2.851	70	0.485	1.853	0.1126	84	1.759	90	1.011	1.601	0.4146
33	6.839	100	0.289	2.583	0.0114	86	3.307	110	0.657	1.967	0.0766
34	2.962	140	0.934	2.524	0.1368	87	4.360	100	0.453	2.255	0.0383
35	2.536	110	0.857	1.853	0.1601	88	4.610	100	0.429	2.242	0.0322
36	1.530	130	1.679	1.707	0.6716	89	3.679	100	0.537	2.158	0.0611
37	3.315	110	0.656	1.976	0.0764	90	2.083	130	1.233	1.777	0.2770
38	2.640	110	0.823	1.893	0.1449	91	3.234	110	0.672	2.113	0.0880
39	1.530	130	1.679	1.707	0.6716	92=8	3.540	110	0.614	2.248	0.0714
40	2.823	110	0.770	2.038	0.1276	93	1.805	130	1.423	1.684	0.4035
43	2.754	140	1.004	2.456	0.1655	94	2.243	110	0.969	1.832	0.2288
45	1.562	150	1.897	1.779	0.6573	95	2.594	110	0.838	1.937	0.1564
47	2.861	140	0.967	2.220	0.1335	96	2.222	130	1.156	1.800	0.2309
48	3.387	140	0.817	2.315	0.0839						

NOTE. — The table contains the running number, the radius of the star, the estimated rotational velocity, estimated rotational frequency, mass, and mean density. The radius and mass used in these estimates were calculated from the spectroscopic parameters using the formulas of Torres et al. (2010), assuming solar metallicity. The same parameters for stars after running numbers 48 can be found in the 7th, 8th, 9th, 10th, 11th, and 12th columns.

spacings.

5.2.1. Midway shift of the sequences

In the framework of the sequence search method we derived the shifts between each pair of sequences as we described in Sec. 3.1. The independent shifts were averaged for the members in the sequence. In the rest of the paper we refer to the average value when we mention the shift. There are two expectations for the shifts. Similar to the spacing in the asymptotic regime, the sequences of the consecutive radial orders of the different l values are shifted relative to each other. For example the $l=0$ and $l=1$ radial orders are shifted to midway between the large separation in the asymptotic regime. The other possible expectation for the shift is the rotational splitting. We checked the shifts of each target for both effects.

Of course, we have shifts only when we found more that one echelle ridge. Only one echelle ridge was found in 20 stars. In 34 stars we have no positive result for the midway shift. However, we found shifts with half of the regular spacing (shifted to midway) in 22 stars. We

present them in Table 7. The table contains the running numbers, the spacing, the numbering of the echelle ridges and the modulo value of the echelle ridges for identification in Figs. 3-10. To follow how precise the midway shift is, we give the deviation in percentage by italics. In some stars there are two pairs with a midway shift (stars No. 8, 71, 72, 74 and 76), while in stars No. 28, 92 and 96 three pairs appear with a midway shift compared to the spacing. Of course, it could happen that the shift to midway represents a 1:2 ratio of the estimated rotational frequency and the spacing, but we mentioned them independently as a similarity to the behavior in the asymptotic regime. In general the ratio of the dominant spacing to the rotational frequency is in the 1.5-4.5 interval for most of our targets (52 stars).

5.2.2. Shift of sequences with the rotational frequency

The pulsation-rotation connection appears in a prominent way when one, two or even more shifts between pairs of the echelle ridges agree with the rotational frequency. We found 31 stars where a doublet, triplet or multiplet

TABLE 7
MIDWAY SHIFTS

Star	Spacing (d^{-1})	No. of ridges (%)	Mod. of ridges
7	1.795	1-2 *(8)*	0.36-0.89
8	2.481	7-8 *(1)*	0.07-0.58
		5-4 *(1)*	0.29-0.79
10	2.614	4-3 *(3)*	0.24-0.76
13	2.674	2-4 *(5)*	0.90-0.37
18	6.001	1-2 *(9)*	0.90-0.35
20	1.478	1-2 *(1)*	0.06-0.57
27	5.995	2-3 *(2)*	0.11-0.62
28	2.655	3-5 *(6)*	0.93-0.22
		4-2 *(11)*	0.05-0.60
		3-6 *(12)*	0.93-0.37
29	2.389	6-4 *(0)*	0.77-0.26
32	1.671	1-3 *(6)*	0.63-0.17
33	2.396	4-3 *(1)*	0.67-0.19
54	2.300	1-2 *(3)*	0.54-0.03
66	2.406	4-2 *(0)*	0.93-0.43
71	3.495	1-4 *(3)*	0.65-0.14
		3-2 *(1)*	0.85-0.34
72	2.249	1-3 *(4)*	0.16-0.68
		2-4 *(9)*	0.43-0.89
74	2.940	7-5 *(5)*	0.64-0.15
		8-2 *(2)*	0.77-0.28
76	1.772	1-3 *(9)*	0.79-0.25
		2-3 *(5)*	0.73-0.25
77	2.521	1-2 *(3)*	0.51-0.04
78	2.392	6-4 *(5)*	0.75-0.22
87	1.867	3-2 *(5)*	0.05-0.54
92	2.576	1-2 *(7)*	0.85-0.31
		3-5 *(1)*	0.13-0.62
		7-6 *(4)*	0.19-0.70
96	2.464	1-7 *(5)*	0.49-0.02
		6-5 *(3)*	0.76-0.27
		3-2 *(3)*	0.92-0.41

NOTE. — The table contains the running numbers, the spacing, the numbering of the echelle ridges and the modulo value of the echelle ridges for identification in Figs. 3-10. The ratio of the shift of the sequences and half of the spacing is given by italics in 3rd column.

appears with a splitting near the rotational frequency. In Table 8 we give the running number of stars, the estimated rotational frequency, the shifts between the sequences, the numbering of echelle ridges connected to each other, and the modulo values of these echelle ridges for identification on Figs 3-10.

Of course, we may not expect that the estimated rotational frequency and the split (shift) of the doublet and the triplet components agree to high precision. As a guideline we followed Goupil et al. (2000) who derived about 30% deviation in the split of the component from the equally-spaced splitting. We accepted the doublets, triplets and multiplets if the deviation of the shifts is less than 20% compared to the estimated rotational frequency. To follow how reliable are the doublets, triplets and multiplets we included the ratio of the actual shift and the estimated rotational frequency. In most cases presented in Table 8 the ratios are even less that 10% (13 stars). We included some examples with higher than 20% representing triplets (stars No. 10, 8 and 93) or complete or incomplete multiplets (stars No. 78 and 92).

For getting a complete view of the connection between the shifts and the estimated rotational frequencies, we included cases where shifts are twice (stars No. 9, 30, 54, 55 and 72) or half (stars No. 8, 29, 66 and 84) the value of the estimated rotational frequency. The devia-

tions are marked by an asterisk in these cases. A missing component in an incomplete multiplet (star No. 87) is also marked by an asterisk.

The attached file to this paper with the flags allows the interested readers to derive the shifts between the pairs of the echelle ridges. The numbering of the flags agrees with the numbering in electronic table.

5.2.3. *Difference of spacings and the rotational frequency*

There are 25 stars in our sample where SSA found more than one spacing between the frequencies (see Table 3). Based on the results obtained for the model frequencies of FG Vir, namely that one of the spacing agrees with the large separation and the other one with the sum of the large separation and the rotational frequency, we generalized how to get the large separation if none of the spacing represent the large separation itself but both spacings are the combination of the large separation and the rotational frequency (Part I paper). We recall the equations:

$$SP_1 = \Delta\nu, \text{ and } SP_2 = \Delta\nu - \Omega_{\text{rot}}, \tag{2}$$
$$SP_2 = \Delta\nu, \text{ and } SP_1 = \Delta\nu + \Omega_{\text{rot}}, \tag{3}$$
$$SP_1 = \Delta\nu + 2\cdot\Omega_{\text{rot}}, \text{ and } SP_2 = \Delta\nu + \Omega_{\text{rot}}, \tag{4}$$
$$SP_2 = \Delta\nu - 2\cdot\Omega_{\text{rot}}, \text{ and } SP_1 = \Delta\nu - \Omega_{\text{rot}}, \tag{5}$$

where, SP_1 and SP_2 are the larger and smaller values of the spacings, respectively, found by SSA, $\Delta\nu$ is the large separation in the traditionally used sense, and Ω_{rot} is the estimated rotational frequency.

The four possible value of the large separation ($\Delta\nu$) are (2) $\Delta\nu = SP_1$, (3) $\Delta\nu = SP_2$ (4) $\Delta\nu = SP_2 - \Omega_{\text{rot}}$ or (5) $\Delta\nu = SP_1 + \Omega_{\text{rot}}$. We applied these equations to the SP_1 and SP_2 spacings of CoRoT 102675756, the star No. 72 of our sample in Part I paper. Obtaining the possible values of the large separation, we plotted them on the mean density versus large separation diagram, along with the relation derived using stellar models by Suárez et al. (2014). We concluded that the most probable value of the large separation is the closest one to the relation.

We applied this concept in this paper to our targets in which the difference of the spacings agrees with the estimated rotational frequency exactly, or nearly, or in which the spacing difference is twice or three times of the rotational frequency. We mentioned the latest group for curiosity, where special relation appears between the estimated rotational velocity. We emphasize that our results are not forced to fulfill the theoretical expectation. To keep the homogeneity we everywhere used the Ω_{rot}, the estimated rotation frequency, to calculate the large separation not the actual difference of the spacings if we have any. In addition to the SSA solutions, we included solution for two stars (No. 47 and 96) from the VI that agreed with the aforementioned requirements. We calculated the four possible large separations for these stars that we present in Table 9. The three groups, concerning the agreement of the difference of the spacings and the rotational frequency, are divided by a line. The columns give the running number, SP_1, SP_2, $SP_1 - SP_2$, Ω_{rot} and the four possible large separations in agreement with the Equations (2), (3), (4) and (5). Fig. 15. shows the location of the best fitting large separations (marked by asterisk in Table 9) on the mean density versus large separation diagram, along with the

Paparó et al.

TABLE 8
Doublets, triplets and multiplets

Star	$\Omega_{\rm rot}$ (d^{-1})	Shift (d^{-1})	No. of ridges	Mod. of ridges
1	0.404	0.455 *(13)*	4-5	0.17-0.39
		0.482 *(19)*	3-2	0.52-0.73
7	0.248	0.224 *(11)*	6-2	0.78-0.89
		0.224-0.563 *(11-14*)*	6-2-5	0.78-0.89-0.22
8	0.614	0.521-0.551 *(18-11)*	6-8-4	0.37-0.58-0.79
		0.325-0.355 *(6*-16*)*	5-2-8	0.29-0.43-0.58
9	0.345	0.664 *(4*)*	3-2	0.91-0.14
10	0.811	0.874 *(8)*	1-2	0.16-0.50
		0.874-0.662 *(8-23)*	1-2-3	0.16-0.50-0.75
13	0.297	0.317 *(7)*	1-2	0.78-0.90
18	1.555	1.430 *(9)*	1-4	0.90-0.15
		1.649 *(6)*	3-2	0.09-0.35
		1.315 *(18)*	4-2	0.15-0.35
		1.430-1.315 *(9-18)*	1-4-2	0.90-0.15-0.35
20	0.727	0.886 *(22)*	3-4	0.30-0.75
27	1.540	1.533 *(0)*	1-4	0.90-0.16
28	0.291	0.308 *(6)*	3-4	0.93-0.05
29	1.037	0.997-1.041 *(4-0)*	1-6-2	0.35-0.77-0.20
		0.546-0.451 *(5*-15*)*	1-7-6	0.35-0.56-0.77
30	0.433	0.459 *(6)*	2-1	0.77-0.91
		0.901 *(4*)*	4-2	0.51-0.77
31	0.648	0.587 *(10)*	1-3	0.64-0.86
32	0.485	0.478 *(1)*	1-4	0.63-0.77
		0.571 *(18)*	3-2	0.17-0.33
33	0.289	0.251 *(15)*	5-3	0.08-0.19
49	1.327	1.568 *(18)*	1-3	0.39-0.05
53	0.402	0.428 *(6)*	4-1	0.48-0.58
		0.361 *(11)*	2-3	0.68-0.80
54	0.341	0.611 *(12*)*	1-3	0.54-0.79
55	0.404	0.818 *(1*)*	2-5	0.45-0.78
		0.729-0.818 *(11*-1*)*	3-2-5	0.17-0.45-0.78
62	1.282	1.277 *(0)*	1-2	0.61-0.92
63	0.630	0.611 *(3)*	4-2	0.67-0.87
66	0.545	0.563 *(3)*	1-4	0.69-0.93
		0.269-0.301 *(1*-10*)*	1-3-4	0.69-0.80-0.93
71	0.747	0.654 *(16)*	1-3	0.65-0.85
		0.672 *(11)*	4-2	0.14-0.34
		0.859 *(15)*	5-6	0.75-0.02
72	0.269	0.603-0.563 *(12*-5*)*	1-2-3	0.16-0.43-0.68
73	1.068	1.247 *(17)*	2-1	0.20-0.57
74	0.297	0.359-0.356-0.346 *(21-20-17)*	4-3-5-2	0.91-0.05-0.15-0.28
76	0.748	0.811-0.844 *(8-13)*	1-3-2	0.79-0.25-0.72
78	0.282	0.364-0.345-0.297-0.361 *(29-22-5-28)*	2-5-4-1-3	0.93-0.11-0.22-0.35-0.50
84	1.011	0.506 *(0*)*	4-2	0.42-0.60
86	0.657	0.610 *(8)*	3-1	0.26-0.32
87	0.453	0.525-0.933-0.406 *(16-3*-12)*	4-2-1-3	0.17-0.54-0.78-0.05
88	0.429	0.357-0.322 *(20-33)*	4-2-1	0.28-0.42-0.54
92	0.614	0.567 *(8)*	4-7	0.96-0.19
		0.605-0.699 *(1-14)*	5-1-3	0.62-0.85-0.13
		0.766-0.605-0.699 *(25-1-14)*	2-5-1-3	0.31-0.62-0.85-0.13
93	1.423	1.285 *(11)*	4-1	0.78-0.10
		1.159-1.285 *(23-11)*	3-4-1	0.51-0.78-0.10
96	1.156	1.123-1.254 *(3-8)*	1-3-2	0.49-0.92-0.41

NOTE. — The table contains the running number, the estimated rotational velocity, the shifts between the rotationally connected echelle ridges, the numbering of echelle ridges connected rotationally, and the modulo value of the echelle ridges for identification purpose on Figs. 3-10.

relation given by Suárez et al. (2014). The three groups are shown by different symbols, and the large separations obtained from different equations are marked by different colors. The stars with $\Delta\nu = SP_1$ (black symbols) perfectly agree with the middle part of the theoretically derived line. These are the stars with intermediate rotational frequency. The stars with higher and lower rotational frequency marked by blue and green symbols and derived by $\Delta\nu = SP_2 - \Omega_{\rm rot}$ and $\Delta\nu = SP_1 + \Omega_{\rm rot}$, respectively, deviate more from the theoretical line. The small black open circles represent $\Delta\nu = SP_2 - 2 \cdot \Omega_{\rm rot}$

(next the green symbols) or $\Delta\nu = SP_1 + 2 \cdot \Omega_{\rm rot}$ values (next the blue symbols).

We found numerical agreement between the difference of the spacings and the rotational frequency only in half of the stars (12 stars) for which SSA found more then one spacings. We do not know why we do not have numerical agreement for the other stars. A reason may be the uncertainties in estimated rotational velocity.

Nevertheless, we proceeded to apply the conclusion based on Equations (2)-(5) deriving the possible large separation to the stars where we do not have an agree-

TABLE 9
POSSIBLE LARGE SEPARATION

No	SP_1 (d^{-1})	SP_2 (d^{-1})	$SP_1 - SP_2$ (d^{-1})	$\Omega_{\rm rot}$ (d^{-1})	(2) (d^{-1})	(3) (d^{-1})	(4) (d^{-1})	(5) (d^{-1})
35	3.492	2.609	0.883	0.857	*3.492	2.609	1.752	4.349
45	3.306	1.407	1.889	1.897	3.306	1.407	–	*5.203
47 (VI)	2.525	1.597	0.928	0.967	2.525	1.597	0.63	*3.492
72	2.249	1.977	0.272	0.269	2.249	1.977	*1.708	2.518
73	3.416	2.417	0.999	1.068	*3.416	2.417	1.349	4.484
95	3.294	2.262	0.832	0.838	*3.294	2.462	1.624	4.132
1	2.092	1.510	0.582	0.404	*2.092	1.510	1.106	2.496
22	2.598	1.877	0.721	0.633	2.598	1.877	1.244	*3.231
92	2.576	1.880	0.696	0.614	*2.576	1.880	1.266	3.190
96 (VI)	3.387	2.429	0.958	1.156	*3.387	2.429	1.273	4.543
9	3.506	2.784	0.722	0.345	3.506	2.784	*2.439	3.851
54	3.275	2.300	0.975	0.341	3.275	2.300	*1.959	3.616

NOTE. — The columns contain the running numbers (No), the spacings, the difference of the spacings, the rotational frequency and the possible large separations in agreement with the Equations (2), (3), (4), and (5).
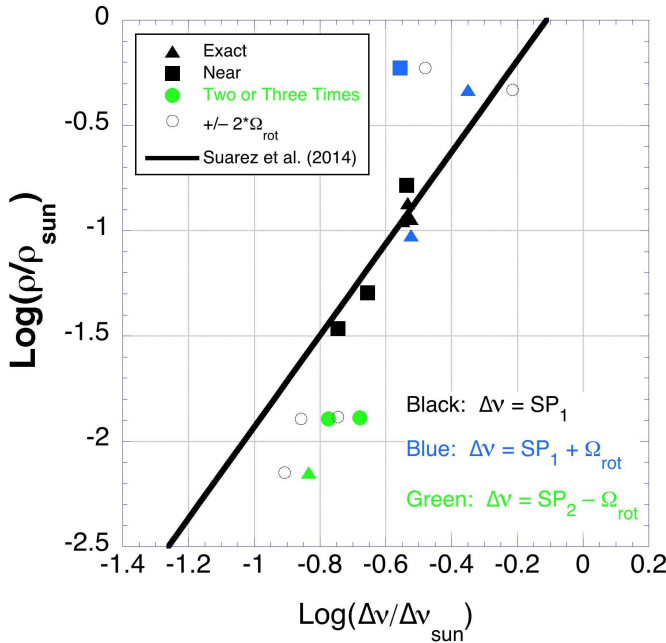

FIG. 15.— Location of the stars on the log mean density vs. log large separation diagram, along with the relation based on stellar models from Suárez et al. (2014). Three groups are those in which the difference of the spacings is: equal to the rotational frequency (triangle); near to that value (square); or twice or three times of the rotational frequency (circles) presented for curiosity. The color code corresponds how the $\Delta\nu$ was calculated: black Eq. (2), green Eq. (4), and blue Eq. (5). Open circles shows $\Delta\nu$ calculated with $\pm 2 \cdot \Omega_{\rm rot}$.
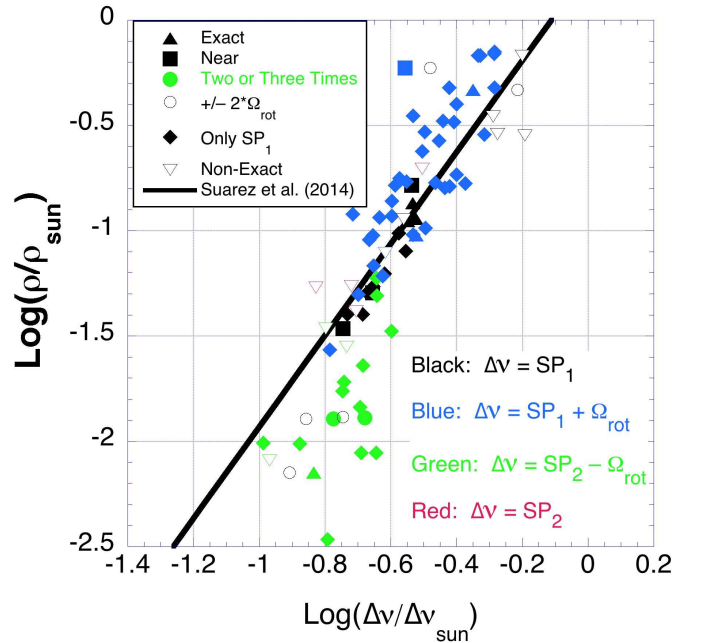

FIG. 16.— Location of the whole sample on the log mean density vs. log large separation diagram, along with the relation based on stellar models from Suárez et al. (2014). The new symbols represent the stars for which there is no agreement between the rotational frequency and the difference of the spacings (inverted triangle) or the stars with only one spacing (diamonds). The color code is the same as in the previous figure, with the addition of the red color corresponding to $\Delta\nu = SP_2$.

ment (14 stars) and to the stars (53) where SSA found only one spacing. Plotting in Fig. 16 the best-fitting value of the large separation for both groups on the mean density versus large separation diagram along with the relation of Suárez et al. (2014), we found that the large separations are closely distributed along the Suárez et al. (2014) line. The figure contains not only the two new groups but the whole sample. Different symbols are used for the two groups (inverted triangle, and diamond, respectively) but the color code according to the calculation of $\Delta\nu$ is kept in the same sense as in Fig. 15. The distribution of the whole sample is consistent. The stars with $\Delta\nu = SP_1$ agree with the middle part of the line,

whether they fulfill the equations or not, although some stars appear with $\Delta\nu = SP_1$ on the upper part of the plot from group with two spacing. The deviation of the stars with higher and lower rotational frequency can be also noticed. We may have a slight selection effect in the lower $\Delta\nu$ region due to the limitation of the spacing search at 1.5 d^{-1}.

We may conclude that we found an unexpectedly clear connection between the pulsational frequency spacings and the estimated rotational frequency in many targets of our sample. The tight connection confirms that our echelle ridges are not frequencies accidentally located along the echelle ridges. They represent the pulsation and rotation of our targets. Of course the well-

determined rotational frequency for as large sample as we have would be needed to confirm the results with higher precision than we have here. However, this way of investigation seems to be a meaningful approach to disentangle the pulsation and rotation in the mostly fast rotating δ Scuti stars.

The frequencies along the ridges could be identified with the island modes in the ray dynamic approach, while frequencies widely distributed in the echelle diagrams could be the chaotic modes. Both of them have observable amplitude in fast rotating stars, but only the island modes show regularity as the echelle ridges (Ouazzani et al. 2015). For the authors it is not trivial to give a deeper interpretation of the results in the ray dynamic approach, but hopefully colleagues will interpret it in forthcoming papers.

6. SUMMARY

We aimed to survey the possible regularities in δ Scuti stars on a large sample in order to determine whether or not we can use the regular arrangement of high precision space-based frequencies for mode identification. Ninety stars observed by the CoRoT space telescope were investigated for regular spacing(s). We introduced the sequence search method with two approaches, the visual inspection and the algorithmic search. The visual inspection supported the parameter range and the tolerance value for quasi-equal spacing. The method proved to be successful in determining the dominant spacing and in finding sequences/echelle ridges in 77 stars stars from one up to nine ridges. Compared to the spacings obtained by SSA and FT we concluded that the different methods (with different requirements) are able to catch different regularities among the frequencies. Not only does the spacing in a sequence represent regularity among the frequencies, but the shift of the sequences, too, can be found.

The sequence search method resulted in very useful parameters beside the most probable spacing, namely the shift of the sequences and the difference of the spacings.

The determination of the averaged shift between the pairs of echelle ridges opens a new field of investigation. With the comparison of the shift to the spacing, we determined one midway shift of at least one pair of the echelle ridges in 22 stars. Comparing the shifts to the es-

timated rotational frequency we recognized rotationally split doublets (in 21 stars), triplets (in 9 stars) and multiplets (in 4 stars) not only for a few frequencies, but for whole echelle ridges in δ Scuti stars that are pulsating in the non-asymptotic regime.

The numerical agreement between the difference of the spacings and the rotational frequency obtained for FG Vir (Part I paper) and in many of our sample stars (12) revealed a possibility for deriving the large separation ($\Delta\nu$) in δ Scuti stars pulsating in the non-asymptotic regime. Generalized to those stars for which there is no numerical agreement between the difference of the spacings with the rotational frequency (14), or for which only one spacing was obtained by SSA (53), we found an arrangement of each target along the theoretically determined mean density versus large separation diagram (Suárez et al. 2014) calculating the $\Delta\nu$ as $\Delta\nu = SP_1$, $\Delta\nu = SP_2$, $\Delta\nu = SP_2 - \Omega_{\rm rot}$ and $\Delta\nu = SP_1 + \Omega_{\rm rot}$. The large separation agrees with the dominant spacing for the stars rotating at intermediate rate. The large separation for sample stars with the higher mean density and fast rotation agrees with $SP_1 + \Omega_{\rm rot}$ and for the stars with lower mean density and slow rotation agrees with $SP_2 - \Omega_{\rm rot}$ (if two spacings were found; otherwise the only spacing was used in the calculation).

The consistent interpretation of our results using the physical parameters of the targets and the agreement with the theoretically expected relation suggest that the unexpectedly large number of echelle ridges represents the pulsation and rotation of our target, and not frequencies accidentally located along the echelle ridges. Although we could not reach at this moment the mode identification level using only the frequencies obtained from space data, this step in disentangling the pulsation-rotation connection is very promising.

The huge database obtained by space missions (MOST, CoRoT and *Kepler*) allows us to search for regular spacings in an even larger sample and provide more knowledge on how to reach the asteroseismological level for δ Scuti stars.

REFERENCES

Aerts, C., Christensen-Dalsgaard, J., & Kurtz, D. W. 2010, Asteroseismology, A&A Library, (Berlin - Heidelberg: Springer)
Auvergne, M., Bodin, P., Boisnard, L., et al. 2009, A&A, 506, 411
Baglin, A., Auvergne, M., Barge, P., et al. 2006, in ESA SP 1306, The CoRoT Mission Pre-Launch Status - Stellar Seismology and Planet Finding, ed. M. Fridlund, A. Baglin, J. Lockhard, & L. Conroy, (ESA), 33
Balona, L. A. 1975, MNRAS, 173, 449
Balona, L. A. & Evers, E. A. 1999, MNRAS, 302, 349
Balona, L. A. 2014, MNRAS, 439, 3453
Balona, L. A., Daszynska-Daszkiewicz, J. & Pamyatnykh, A. A. 2015, MNRAS, 437, 1476
Benkő, J. M., & Paparó, M. 2015, in Astronomy in Focus 1, FM17 – Advances in Stellar Physics from Asteroseismology, ed. S. Jeffery & J. A. Guzik, (IAU), in press
Borucki, W. J., Koch, D., Basri, G., et al. 2010, Science, 327, 977
Breger, M., Pamyatnykh, A. A., Pikall, H., & Garrido, R. 1999, A&A, 341, 151

Breger, M., Lenz, P., Antoci, V., et al. 2005, A&A, 435, 955
Breger, M., & Lenz, P. 2008, A&A, 488, 643
Breger, M., Lenz, P., & Pamyatnykh, A. A. 2009, MNRAS, 396, 291
Breger, M., Balona, L., Lenz, P., et al. 2011, MNRAS, 414, 1721
Breger, M., Fossati, L., Balona, L., et al. 2012, ApJ, 759, 62
Debosscher, J., Sarro, L. M., López, M., et al. 2009, A&A, 506, 519
Dziembowski, W. A. & Goode, P. 1992, ApJ, 394, 670
García Hernández, A., Moya, A., Michel, E. et al. 2009, A&A, 506, 79
García Hernández, A., Moya, A., Michel, E. et al. 2013, A&A, 559, A63
García Hernández, A., Lignières, F., Balona, L., et al. 2015, in EPJ Web of Conf. 101, The Space Photometry Revolution, ed. R. A. García, & J. Ballot, id.06026

Garrido, R. 2000, in ASP Conf. Ser. 210, Delta Scuti and Related Stars, ed. M. Breger & M. H. Montgomery, (San Francisco, CA: ASP), 67

Glebocki, R. & Stawikowski, A. 2000, AcA, 50, 509

Goupil, M.-J., Dziembowski, W. A., Pamyatnykh, A. A., & Talon, S. 2000, in ASP Conf. Ser. 210, Delta Scuti and Related Stars, ed. M. Breger & M. H. Montgomery, (San Francisco, CA: ASP), 267

Guenther, E. W., Gandolfi, D., Sebastian, D., et al. 2012, A&A, 543, A125

Handler, G., Pikall, H., O'Donoughue, D., et al. 1997, MNRAS, 286, 303

Hareter, M. 2013, PhD Thesis, Univ. Vienna, Austria

Kurtz, D. W., Saio, H., Takata, M., et al. 2014, MNRAS, 444, 102

Ledoux, P. 1951, ApJ, 114, 373

Lignières, F., Rieutord, M., & Reese, D. R. 2006, A&A, 455, 607

Lignières, F., & Georgeot, B. 2008, Phys. Rev. E, 78, 6215

Lignières, F., & Georgeot, B. 2009, A&A, 500, 1173

Lignières, F., Georgeot, B., & Ballot, J. 2010, Astron. Nachr., 331, 1053

Mantegazza, L., Poretti, E., & Bossi, M. 1994, A&A, 287, 95

Mantegazza, L., Poretti, E., Michel, E., et al. 2012, A&A, 542, A24

Matthews, J. M. 2007, CoAst, 150, 330

Moya, A., García Hernández, A., Suárez, J.-C. et al. 2010, astro-ph: 1004.0100v1

Ouazzani, R.-M., Roxburgh, I. W., & Dupret, M.-A. 2015, A&A, 579, A116

Pamyatnykh, A. A., Dziembowski, W. A., Handler, G., & Pikall, H. 1998, A&A, 333, 141

Paparó, M., Bognár, Zs., Benkő, J. M., et al. 2013, A&A, 557, A27

Paparó, M., Benkő, J. M., Hareter, M., & Guzik, J. A. 2015, ApJ, submitted (Paper I)

Poretti, E., Rainer, M., Weiss, W. W., et al. 2011, A&A, 528, A147

Reegen, P. 2007, A&A, 467, 1353

Reese, D. R., Lignières, F., & Rieutord, M. 2006, A&A, 455, 621

Reese, D. R., Lignières, F., & Rieutord, M. 2008, A&A, 481, 449

Reese, D. R., Thompson, M. J., MacGregor, K. B., et al. 2009, A&A, 506, 183

Rodríguez, E., Fauvaud, S., Farrell, J. A., et al. 2007, A&A, 471, 255

Roxburgh, I. W. 2006, A&A, 454, 883

Sebastian, D., Guenther, E. W., Schaffenroth, V., et al. 2012, A&A, 541, A34

Soufi, F., Goupil, M.-J., & Dziembowski, W. A. 1998, A&A, 334, 911

Suárez, J. C., García Hernández, A., Moya, A., et al. 2014, A&A, 563, A7

Templeton, M. R., Bradley, P. A. & Guzik, J. A. 2000, ApJ, 528, 979

Templeton, M. R., Basu, S., & Demarque, P. 2001, ApJ, 563, 999

Torres, G., Andersen, J., & Giménez, A. 2010, A&A Rev., 18, 67

Unno, W., Osaki, Y., Ando, H, et al. 1981, Nonradial Oscillations of Stars, (Tokyo: Univ. of Tokyo Press), 2nd ed.

Viskum, M., Kjeldsen, H., Bedding, T., et al. 1998, A&A, 335, 549

Vorontsov, S. V. 1981, Soviet Astron., 25, 724

Vorontsov, S. V. 1983, Sol. Phys., 82, 379

Watson, R. D. 1988, Ap&SS, 140, 255